Radiology

Advances in Imaging of Osteoarthritis and Cartilage[1]

Frank W. Roemer, MD
Michel D. Crema, MD
Siegfried Trattnig, MD
Ali Guermazi, MD

Online CME
See www.rsna.org/ry_cme.html

Learning Objectives:

After reading this article and taking the test, the reader will be able to:

- Discuss the role of different imaging modalities in the assessment of osteoarthritis (OA), including radiography, US, and MR imaging.
- Summarize different MR techniques for the evaluation of articular cartilage and OA imaging.
- Describe MR imaging–based outcome measures for the evaluation of OA, including semiquantitative morphologic, quantitative three-dimensional, and biochemical approaches.
- Discuss the importance of MR imaging and compositional MR techniques in the follow-up of cartilage repair procedures.

Accreditation and Designation Statement

The RSNA is accredited by the Accreditation Council for Continuing Medical Education (ACCME) to provide continuing medical education for physicians. The RSNA designates this journal-based CME activity for a maximum of 1.0 *AMA PRA Category 1 Credit*™ . Physicians should only claim credit commensurate with the extent of their participation in the activity.

Disclosure Statement

The ACCME requires that the RSNA, as an accredited provider of CME, obtain signed disclosure statements from authors, editors, and reviewers for this activity. For this journal-based CME activity, author disclosures are listed at the end of this article. The editor and the reviewers indicated that they had no relevant relationships to disclose.

[1] From the Quantitative Imaging Center, Department of Radiology, Boston University School of Medicine, 820 Harrison Ave, FGH Building, 3rd Floor, Boston, MA 02118 (F.W.R., M.D.C., A.G.); Department of Radiology, Klinikum Augsburg, Augsburg, Germany (F.W.R.); Institute of Diagnostic Imaging and Division of Radiology, University of São Paulo at Ribeirão Preto, Ribeirão Preto, SP, Brazil (M.D.C.); and MR Center of Excellence, Department of Radiology, Medical University of Vienna, Vienna, Austria (S.T.). Received July 15, 2010; revision requested September 3; revision received October 17; accepted November 17; final version accepted November 20. **Address correspondence to** F.W.R. (e-mail: *froemer@bu.edu*).

Osteoarthritis (OA) is the most frequent form of arthritis, with major implications for individual and public health care without effective treatment available. The field of joint imaging, and particularly magnetic resonance (MR) imaging, has evolved rapidly owing to technical advances and the application of these to the field of clinical research. Cartilage imaging certainly is at the forefront of these developments. In this review, the different aspects of OA imaging and cartilage assessment, with an emphasis on recent advances, will be presented. The current role of radiography, including advances in the technology for joint space width assessment, will be discussed. The development of various MR imaging techniques capable of facilitating assessment of cartilage morphology and the methods for evaluating the biochemical composition of cartilage will be presented. Advances in quantitative morphologic cartilage assessment and semiquantitative whole-organ assessment will be reviewed. Although MR imaging is the most important modality in imaging of OA and cartilage, others such as ultrasonography play a complementary role that will be discussed briefly.

Supplemental material: *http://radiology.rsna.org/lookup/suppl/doi:10.1148/radiol.11101359/-/DC1*

Osteoarthritis (OA) is the most prevalent form of arthritis, with major implications for individual and public health care (1–3). Its prevalence is expected to increase with the growing obesity epidemic and the aging baby-boomer population (4,5). To date, there is still no effective treatment for OA, which reflects the lack of understanding of the pathophysiology and natural history of the disease.

OA is viewed today as the clinical and pathologic outcome of a range of disorders that result in structural and functional failure of synovial joints (6). OA occurs when the dynamic equilibrium between the breakdown and repair of joint tissues is overwhelmed, which eventually will cause pain, physical disability and psychologic distress (7). The inflammatory changes in OA are probably secondary to soluble breakdown of cartilage and bone, and most researchers today consider the disease to be not a passive degenerative disorder but rather an active disease process driven primarily by mechanical factors (8). Other factors such as genetic predisposition and metabolic and, possibly, vascular abnormalities (9,10) seem to play an important role, especially in the initiation of the disease process.

Since OA is a slowly progressive disorder, OA clinical trials require large cohorts that must be followed up for many years (11). For these reasons, many pharmaceutical companies and basic researchers have been moving out of the field in recent years (12).

However, the application of sophisticated imaging methods has led to a rapid increase in knowledge, and large longitudinal studies are adding to our understanding of the disease's natural course. The Osteoarthritis Initiative, a private-public partnership of the National Institutes of Health and several pharmaceutical companies *(http://www.niams.nih.gov/ne/oi/),* is ongoing and is one of the first large studies with data that are publicly available, including 3-T magnetic resonance (MR) imaging data acquired at multiple time points. With almost 5000 participants followed up for at least 5 years, the research community is hoping for a break-through in answering many of the unresolved issues in the OA enigma.

At the same time, the field of imaging, and particularly MR imaging, has evolved rapidly owing to technical advances and the application of these advances to the clinical research arena. In the context of joint imaging, cartilage imaging is at the forefront of these developments. Compositional MR imaging of cartilage ultrastructure has given us a deeper understanding of the early and potentially reversible pathologic processes, which may eventually allow us to prevent the long-term health burden of OA.

This article will review the different aspects of OA imaging and cartilage assessment, especially with regard to recent advances. Because the majority of research in OA and cartilage imaging is focused on the knee joint, the focus of this review will also be the knee. We will review the current role of radiography and present advances in the technology of the assessment of joint space width (JSW). In light of novel therapeutic options for cartilage damage on a surgical and pharmacologic level, we will further detail the development of various MR imaging techniques that can help assess cartilage morphology; in addition, we will discuss methods for evaluating the biochemical composition of cartilage. Advances in quantitative morphologic cartilage assessment have made large and important contributions to our understanding of disease progression in recent years and will be presented in detail.

OA has been regarded as a disease of "wear and tear" for a long time. Recently, however, and largely owing to the application of MR imaging in large clinical studies, a change in paradigm has occurred in that a consensus has developed to perceive OA not simply as a disease of cartilage, but as a whole-organ disorder involving multiple joint tissues and leading to eventual joint failure. Whole-organ assessment has contributed much to this change in perception, and we will discuss in detail the role of the different joint structures in a clinical context and their relevance for disease progression.

Although MR imaging is the most important method for imaging of OA and cartilage, other modalities such as ultrasonography (US) play an important complementary role that will be discussed briefly. Since there is only limited

Essentials

- Radiography is still the first-line diagnostic tool in osteoarthritis and may be used for patient stratification in clinical trials, but it is insensitive to change and does not depict soft tissue sufficiently.
- Whole-organ semiquantitative MR imaging-based knee assessment is a reliable instrument to evaluate all tissues involved in the osteoarthritic disease process and may be applied in cross-sectional and longitudinal studies.
- Several new techniques to depict cartilage with MR imaging are available, including 3D fast spin-echo and high-field-strength (up to 7-T) systems.
- Quantitative 3D cartilage morphometry is a validated and reliable tool to assess several cartilage parameters cross sectionally and in a longitudinal fashion and is complementary to other evaluation techniques.
- Compositional MR imaging might play an important role in the assessment of early and potentially reversible cartilage damage, and several techniques are available and applicable in a clinical setting.

Published online
10.1148/radiol.11101359 **Content codes:** MK MR

Radiology 2011; 260:332–354

Abbreviations:
DESS = dual-echo steady-state
dGEMRIC = delayed gadolinium-enhanced MR imaging of cartilage
FSE = fast spin echo
GAG = glucosaminoglycan
JSW = joint space width
OA = osteoarthritis
SPGR = spoiled gradient-recalled echo
3D = three-dimensional
2D = two-dimensional

Potential conflicts of interest are listed at the end of this article.

knowledge on the application of fluoride 18–fluorodeoxyglucose positron emission tomography and computed tomography in osteoarthritis imaging in a clinical and research setting, these modalities will not be covered in this review.

The field of imaging in OA and cartilage has evolved rapidly, and, despite the continued lack of effective therapies, there is hope that imaging might be in a position to help drive a therapeutic breakthrough.

Role of Radiography and Recent Developments

Traditionally, OA structural changes have been assessed with radiographs. Radiography is used in clinical practice to establish the diagnosis of OA and to monitor the progression of the disease. Radiographs depict bony features, including marginal osteophytes, subchondral sclerosis, and subchondral cysts, that are associated with OA and provide an indirect estimate of cartilage thickness and meniscal integrity by allowing assessment of JSW. Radiographic assessment of OA relies mainly on the evaluation of both osteophytes and joint space narrowing. Osteophytes develop at an earlier stage than joint space narrowing, and they are the most widely applied radiographic criterion for defining the presence of OA, while assessment of the severity of OA relies mainly on joint space narrowing and concomitant subchondral bone abnormalities (13–15). The main shortcomings of radiography are its insensitivity to change and its lack of soft-tissue depiction.

The severity of radiographic OA can be estimated by using semiquantitative scoring systems. Published atlases (16–18) provide example images that represent specific grades. Several grading scales that incorporate combinations of features have also been developed, including the most widely used Kellgren-Lawrence grading scheme, which is the current accepted standard for the diagnosis of OA on radiographs (15,19) (Table 1). The definition of radiographic OA relies on the presence of "definite" osteophytes on the anteroposterior weight-bearing radiograph (Kellgren-Lawrence grade 2). The differentiation between grades 2 and 3 is based on the presence of joint space narrowing. The Kellgren-Lawrence scoring system is limited by the invalid assumption that radiographic changes appear in a linear fashion over the course of the disease and that it is a composite measure of JSW and osteophyte presence. In contrast, the Osteoarthritis Research Society International atlas classification uses scores based on tibiofemoral joint space narrowing and osteophytes separately in each compartment of the knee (16).

The relationship between radiographic progression of joint space narrowing and cartilage loss seen on MR images in patients with symptomatic knee OA and MR imaging–based cartilage loss and its relation to radiographic progression was investigated by Amin and co-workers (20), who showed that a substantial proportion of knees exhibit cartilage loss on MR images even when no radiographic progression is observed. Radiographic progression appeared specific (91%) but not sensitive (23%) for cartilage loss (Fig 1).

For decades, the extended-knee radiograph (ie, bilateral weight-bearing anteroposterior view of both knees in full extension) has been the standard radiograph used to visualize the tibiofemoral joint (21). While the diagnostic utility of the extended-knee radiograph is established, this technique has limits with regard to reproducibility in longitudinal assessments of the joint space (22).

Several research groups have developed alternative protocols for standardized positioning of the knee. Common to all of these techniques is a standard of knee flexion, rather than extension, that provides contact between the tibia and the posterior aspect of the femoral condyle (23). The protocols differ, however, with respect to the degree of flexion required, the angulation of the x-ray beam, and the parameter that is adjusted to meet the positioning standards of the examination. For some positioning protocols, fluoroscopy is used to confirm satisfactory anatomic positioning of the medial tibial plateau prior to acquisition of the radiograph, while for others a nonfluoroscopic positioning standard is used (ie, semiflexed metatarsophalangeal and fixed flexion views) (24–27).

Measurement of JSW is the prerequisite for assessment of joint space narrowing in clinical trials. Prior to the development of automated and semiautomated methods, JSW was measured by using purely manual methods (28,29). Although manual methods offer simplicity of equipment and application and can be used to measure any linear distance, they are time consuming, subjective, and very labor intensive.

Automated and semiautomated techniques for use in clinical trials have been developed to provide rapid, objective, and precise measurements of JSW. Most of the work has been aimed at using automation to improve reproducibility of semiquantitative scoring or manual measurements. Different measures of joint space width have been introduced, including minimum JSW, mean JSW, or joint space area and location-specific JSW. Minimum JSW is defined as the shortest distance between the tibial and femoral margins of the joint space within the weight-bearing areas of the medial and lateral tibiofemoral compartments. In addition, newer methods, known as statistical shape models, have been introduced to segment the anatomy of the knee joint on radiographs (30,31). This approach uses multivariate statistics to derive the allowable shape of an object from a set of examples.

Determination of mean JSW or joint space area has been studied in either a constant area or a region of interest, and its utility has been compared with that of minimum JSW. Minimum JSW was found to be more reproducible and more sensitive to change than is mean JSW or joint space area (32,33). While the most generally used and accepted outcome measurement to determine OA progression is minimum JSW, location-specific JSW measurement might offer advantages concerning reproducibility and responsiveness (29,34–36).

The advances in standardized knee radiography that have made clinical trials of disease-modifying OA drugs feasible can also benefit clinical practice. As noted earlier, the conventional extended-knee

Table 1

Overview of Kellgren-Lawrence Grading System for Assessment of Radiographic OA

Kellgren-Lawrence Grade	Definition*
0	No feature of OA
1	Doubtful JSN and possible osteophytic lipping
2	Definite osteophytes and possible JSN
3	Moderate multiple osteophytes, definite JSN, and some sclerosis and possible deformity of bone ends
4	Large osteophytes, marked JSN, severe sclerosis, and definite deformity of bone ends

Source.—Reference 15.

Note.—Radiographic OA is defined as Kellgren-Lawrence grade 2.

*JSN = joint space narrowing.

radiograph is still used by clinicians to document evidence of marginal tibiofemoral osteophytes on which the diagnosis of knee OA is based. However, the radiographic severity of knee OA (ie, the extent of joint space narrowing in the presence of marginal osteophytes) may not be apparent on the extended-knee view (22,37). Most clinical radiology departments are capable of producing a posteroanterior radiograph of the knee in the Lyon-Schuss position with 10° caudad angulation of the x-ray beam (ie, a fixed-flexion radiograph, with or without use of a positioning frame) (Fig 2). A radiograph satisfying these standards would offer two distinct advantages over the conventional extended-knee view. First, knee flexion is more likely to reveal cartilage loss that is common to the posterior aspect of the femur (23). Second, the fixed-flexion view is more likely than the extended-knee view to represent the joint space in parallel or near-parallel alignment with the x-ray beam. These strengths promise greater accuracy in evaluation of the severity of structural changes of tibiofemoral OA and may result in an image of the knee that likely will be more reliably reproduced during future assessments of disease progression.

The Role of MR Imaging

MR Imaging–based Whole-Joint Assessment of Knee OA with Semiquantitative Scoring Methods

Semiquantitative morphologic whole-organ scoring was originally introduced in 1999 (38) and has since been applied to a multitude of OA studies. The knee joint is assumed to represent an organ, because it is composed of multiple tissues whose integrity is essential for the joint to function optimally. The analyses based on semiquantitative scoring have added much to the understanding of the pathophysiology and natural history of OA, as well as the clinical implications of the structural changes assessed (39–48).

While these scoring systems are not commonly applied in a clinical setting, knowledge of currently available scoring schemes is helpful for any researcher or clinician potentially interested in engaging in image analysis of publicly available MR imaging data sets. In a clinical setting, cartilage is routinely assessed with modified classifications of the Outerbridge scale that take into account depth of a cartilage lesion. Since these systems have flaws related to the lack of accounting for areal extent of the lesion, we emphasize alternative scoring attempts that might also be helpful clinically. A variety of features are assessed that are currently believed to be relevant to the functional integrity of the knee, are potentially involved in the pathophysiology of OA, or both. These articular features include articular cartilage integrity, subarticular bone marrow abnormalities, subchondral cysts, subarticular bone attrition, marginal and central osteophytes, meniscal integrity and extrusion, anterior and posterior cruciate ligament integrity, medial and lateral collateral ligament integrity, synovitis and effusion, and intraarticular loose bodies, as well as periarticular cysts and bursitis.

Whole-organ assessment with scoring of different joint structures on MR images has shown adequate reliability, specificity, and sensitivity, as well as an ability to demonstrate lesion progression (44,49–51) (Table 2).

To date, three semiquantitative scoring systems for whole-organ assessment of knee OA have been published: the Whole-Organ Magnetic Resonance Imaging Score (51), the Knee Osteoarthritis Scoring System (50), and the Boston Leeds Osteoarthritis Knee Score (49). Additional scoring tools have been introduced to cover joint conditions that may not be adequately assessed with the above systems or that offer alternative approaches. Examples are the assessment of synovitis on contrast material–enhanced MR images or detailed evaluation of the intercondylar tibial region (52,53). An overview of the three whole-organ scoring systems is presented in Table 3.

A detailed description of the available semiquantitative scoring systems is presented in Appendix E1 (online).

MR Imaging Techniques for Morphologic Assessment of Cartilage

Several MR imaging techniques are available to facilitate the assessment of cartilage morphology in the knee. Each of them has strengths and weaknesses that need to be considered (Table 4).

In general, fat suppression is useful in cartilage imaging because it results in a higher dynamic range of signal intensities

Figure 1

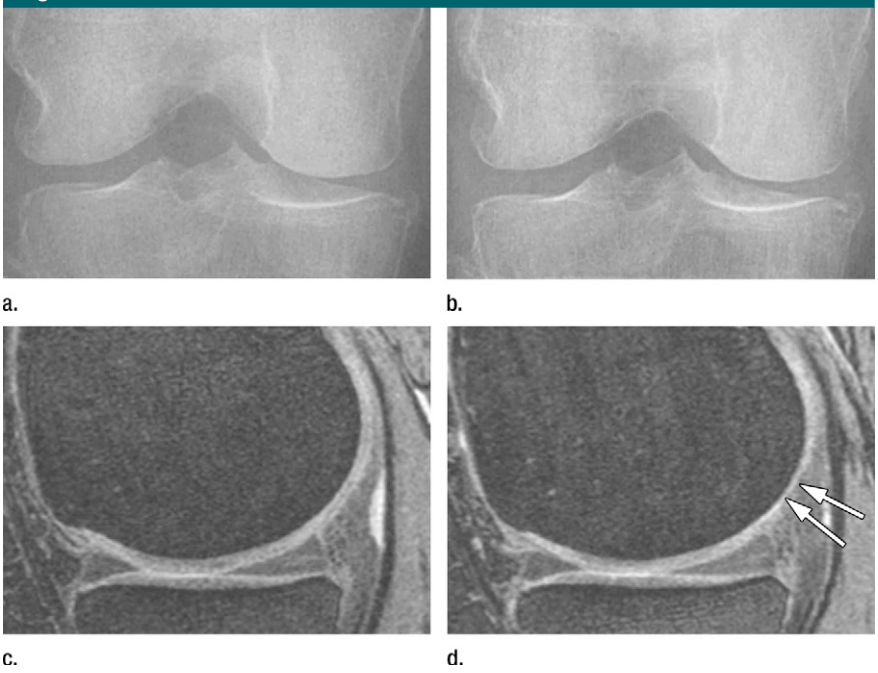

Figure 1: Sensitivity to change. Comparison of baseline and 24-month follow-up imaging examinations. **(a, b)** Anteroposterior radiographs **(a)** show no joint space narrowing at baseline but a definite medial tibial osteophyte and **(b)** no change in JSW at 24 months and slight increase in size of the medial tibial osteophyte. **(c, d)** Sagittal three-dimensional (3D) dual-echo steady-state (DESS) MR images (repetition time msec/echo time msec, 16.3/4.7; flip angle, 25°) show **(c)** no cartilage loss in medial tibiofemoral compartment at baseline but **(d)** definite cartilage damage in posterior medial femur at 24-month follow-up. The damage can only be visualized on MR images due to the posterior location (arrows) of the cartilage abnormality.

Figure 2

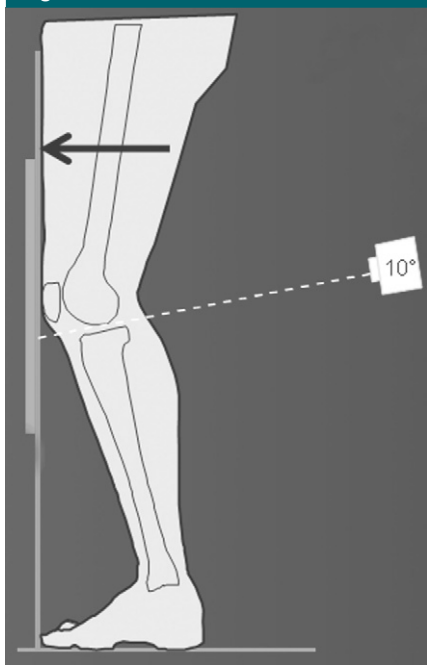

Figure 2: Schematic of patient positioning for fixed-flexion posteroanterior view. Both knees are in contact with the cassette and are coplanar with hips, patellae, and tips of the great toes. Fixed-flexion technique requires x-ray beam be directed 10° caudad.

in the articular cartilage and reduces or eliminates chemical shift artifacts.

Fat saturation is most commonly used, although it increases acquisition times and is very sensitive to magnetic field inhomogeneities. As an alternative to achieving high contrast between sucbchondral bone and cartilage, rapid water excitation MR imaging has been applied with commonly used gradient-recalled-echo techniques and is used especially in volumetric approaches of cartilage assessment (54–57). The principle is the selective excitation of non–fat-bound protons, which obviates the time-consuming spectral fat-saturation prepulse. Iterative decomposition of water and fat with echo asymmetry and least-squares estimation and short tau inversion-recovery imaging are good options for cartilage assessment; they provide uniform lipid suppression in areas of magnetic field inhomogeneity (58–60).

In a clinical setting, 2D proton density–weighted or T2-weighted fat-suppressed FSE sequences are most commonly applied in imaging of knee cartilage and the knee joint in general. The use of intermediate-weighted sequences that mix proton density and T2 contrast by using echo times of 33–60 msec may be useful, because such sequences provide higher intrinsic cartilaginous contrast than does a pure T2-weighted sequence and are less susceptible to "magic-angle" effects seen in techniques with shorter echo times (61). However, 2D FSE techniques suffer because they produce anisotropic voxels, section gaps, and partial-volume effects. Recently, 3D FSE sequences with isotropic resolution have been introduced that exhibit signal intensity characteristics similar to those achieved with intermediate-weighted sequences (Fig 3). Three-dimensional FSE imaging can provide high-quality multiplanar reformations, which are potentially useful not only for the assessment of cartilage morphology, but also for the evaluation of the menisci, cruciate ligaments, and subchondral bone (62,63). Three-dimensional FSE is a promising technique for knee OA trials, because it substantially reduces assessment time compared with that of routine protocols.

Three-dimensional FSE sampling perfection with application-optimized contrast using different flip-angle evolutions (or SPACE) can be acquired with isotropic voxels and demonstrates better signal-to-noise ratio and signal-to-noise ratio efficiency, compared with other 3D techniques commonly used to assess cartilage (64). However, its shortcomings include long acquisition times and poor cartilage-to-fluid contrast; also, its ability to show distinctions between cartilage and other surrounding tissues was shown to be inferior to that of other techniques (64).

Table 2

Inter- and Intrareader Reliability Results from the Literature for MR Imaging Features That Use Different Whole-Joint Scoring Systems

Joint Feature	BLOKS (49) Interreader (weighted κ)*	KOSS (50) Interreader (ICC*, weighted κ)	KOSS (50) Intrareader (ICC*, weighted κ)	WORMS (51) Interreader Agreement (ICC)
Cartilage morphology	0.72 (0.59, 0.85)	0.64 (0.58, 0.69), 0.57	0.78 ([0.74, 0.81), 0.67	0.99
Cartilage 2 (BLOKS only)	0.73 (0.60, 0.85)	Not applicable	Not applicable	Not applicable
Osteochondral defects (KOSS only)	Not applicable	0.63 (0.55, 0.70), 0.66	0.87 (0.83, 0.90), 0.87	Not applicable
Bone marrow lesion size	0.72 (0.58, 0.87)	0.91 (0.88, 0.93), 0.88	0.93 (0.91, 0.94), 0.91	0.74
Bone marrow lesion percentage area (BLOKS only)	0.69 (0.55, 0.82)	Not applicable	Not applicable	Not applicable
Percentage of lesion bone marrow lesion (BLOKS only)	0.72 (0.58, 0.87)	Not applicable	Not applicable	Not applicable
Osteophytes	0.65 (0.52, 0.77)	0.71 (0.67, 0.76), 0.67	0.76 (0.72, 0.80), 0.79	0.97
Synovitis	0.62 (0.05, 1.00)	0.74 (0.58, 0.85), 0.69	0.81 (0.69, 0.89), 0.77	0.74
Effusion	0.61 (0.05, 0.85)	Scores combined†	Scores combined†	Scores combined†
Meniscal extrusion or subluxation	0.51 (0.24, 0.78)	0.67 (0.57, 0.75), 0.65	0.82 (0.75, 0.86), 0.82	Not applicable
Meniscal signal intensity and/or intrasubstance degeneration	0.68 (0.44, 0.93)	0.78 (0.68, 0.85), 0.66	0.76 (0.66, 0.83), 0.56	Not applicable
Meniscal tear	0.79 (0.40, 1.00)	0.70 (0.61, 0.77), 0.70	0.78 (0.70, 0.83), 0.78	0.87
Ligaments	Not applicable	Not applicable	Not applicable	1.0
Subchondral cysts	Part of bone marrow lesion percentage score	0.87 (0.83, 0.89), 0.83	0.90 (0.87, 0.92), 0.87	0.94
Baker cysts	Not applicable	0.89 (0.76, 0.95), 0.80	0.96 (0.90, 0.98), 0.91	Not applicable

Note.—BLOKS = Boston Leeds Osteoarthritis Knee Score, ICC = intraclass correlation coefficient, KOSS = Knee Osteoarthritis Scoring System, WORMS = Whole-Organ Magnetic Resonance Imaging Score.

*Data in parentheses are the 95% confidence interval.

†Scores were combined with those from the Synovitis row above.

Three-dimensional SPGR imaging is considered the standard for quantitative morphologic assessment of knee cartilage because of its excellent diagnostic accuracy when compared with arthroscopy (65–68). This MR technique has been widely used in studies in which segmentation techniques were used, with cartilage morphometry as the outcome owing to high spatial resolution and very high signal intensity of the articular cartilage (69–72). Disadvantages inherent to 3D SPGR include lack of reliable contrast between cartilage and fluid; inability to assess other knee structures such as ligaments, menisci, or subchondral bone; long imaging times; and high sensitivity to susceptibility artifacts.

Three-dimensional DESS imaging is another commonly used technique for morphologic assessment of knee cartilage (55,73–75) (Fig 4). Compared with 3D SPGR, 3D DESS imaging is more time efficient and has higher signal-to-noise ratio and higher cartilage-to-fluid contrast (76). In knee OA trials, 3D DESS imaging allowed quantitative 3D assessment of cartilage with good accuracy and precision (55). Compared with other 3D gradient-recalled-echo techniques, 3D DESS exhibits similar longitudinal sensitivity to change of cartilage thickness measurements (77).

Although 3D gradient-recalled-echo types of techniques were developed for dedicated cartilage imaging, the relatively poor contrast between cartilage and joint fluid they yield renders them inferior for depicting focal cartilage defects, as compared with standard 2D FSE techniques (78–82) (Fig 5).

Three-dimensional isotropic balanced steady-state free precession (SSFP) MR imaging provides excellent synovial fluid-to-cartilage contrast (83). This technique has good diagnostic performance in the assessment of knee cartilage morphology, similar to that of routine MR imaging and other commonly used 3D GRE imaging protocols (54,84,85) (Fig 6). In addition, 3D balanced SSFP imaging has been shown to be useful for imaging of other internal knee structures such as ligaments and menisci, making its implementation in knee OA trials an interesting choice (86). Recently, a technique that combines balanced SSFP imaging with a 3D radial k-space acquisition termed *vastly interpolated projection reconstruction* (or VIPR-SSFP) has been reported. This sequence yields images of the knee with isotropic resolution and excellent diagnostic performance regarding detection of cartilaginous, meniscal, and ligamentous lesions in the knee, as well as associated changes in bone marrow (87).

Three-dimensional driven-equilibrium Fourier transform (DEFT) imaging provides good contrast between fluid and cartilage. Its diagnostic performance in the detection of cartilage lesions in

Table 3

Comparison of Semiquantitative Scoring Systems for Knee OA

Parameter	WORMS	KOSS	BLOKS
No. of knees scored in original study	19	25	10 (plus 71 for validity exercise of BML scoring)
MR imaging protocol in original study (all with 1.5-T systems)	Axial, coronal, and sagittal T1-weighted spin-echo; sagittal T2 weighted with fat suppression and 3D SPGR	Coronal and sagittal T2 weighted and proton density weighted, sagittal 3D SPGR, axial proton density weighted and axial T2 weighted with fat suppression	For reliability exercise (10 knees): sagittal and coronal T2 weighted with fat suppression, sagittal T1-weighted spin echo, and axial and coronal 3D fast low-angle shot; for validity of BML assessment: sagittal proton density and T2 weighted; and coronal and axial proton density and T2 weighted with fat suppression
Subregional division of knee	15 Subregions: medial and lateral patella, medial and lateral femur (anterior, central, posterior), medial and lateral tibia (anterior, central, posterior), subspinous tibia	9 Subregions: medial patella, patellar crest, lateral patella, medial and lateral trochlea, medial and lateral femoral condyle, medial and lateral tibial plateau	9 Subregions: medial and lateral patella, medial and lateral trochlea, medial and lateral weight-bearing femur, medial and lateral weight-bearing tibia, subspinous tibia
Interreader reliability	In 19 knees: ICC of 0.74 (bone marrow abnormalities and synovitis or effusion) and 0.99 (cartilage)	In 25 knees: weighted κ of 0.57 (osteochondral defects) and 0.88 (bone marrow edema)	In 10 knees: weighted κ of 0.51 (meniscal extrusion) and 0.79 (meniscal tear)
Intrareader reliability	Not reported	In 25 knees: weighted κ of 0.56 (intrasubstance meniscal degeneration) and 0.91 (bone marrow edema and Baker cyst)	Not reported
Scored MR Features			
Bone marrow lesions	Summed BML size and volume from 0 to 3 for subregion in regard to percentage of subregional bone volume	Scoring of individual lesions from 0 to 3 concerning maximum diameter of lesion	Scoring of individual lesions; 3 aspects of BMLs are scored: *(a)* size of BML scored from 0 to 3 in regard to percentage of subregional bone volume, *(b)* percentage of surface area adjacent to subchondral plate, and *(c)* percentage of BML that is noncystic
Cartilage	Subregional approach: scores from 0 to 6 depending on depth and extent of cartilage loss; intrachondral cartilage signal intensity additionally scored as present or absent	Subregional approach: focal and diffuse defects are differentiated; depth of lesions scored from 0 to 3; diameter of lesion scored from 0 to 3; osteochondral defects scored separately	Score 1: subregional approach; *(a)* percentage of any cartilage loss in subregion; *(b)* percentage of full-thickness cartilage loss in subregion; score 2: site-specific approach, with score from 0 (none) to 2 (full-thickness loss) of cartilage loss at 11 specific locations (not subregions)
Subchondral cysts	Summed cyst size and volume for subregion scored from 0 to 3 in regard to percentage of subregional bone volume	Individual lesion scored from 0 to 3 in regard to maximum diameter of lesion.	Scored together with BMLs
Osteophytes	Scored from 0 to 7 at 16 sites	Scored from 0 to 3; marginal, intercondylar, and central osteophytes are differentiated; locations or sites of osteophyte scoring not forwarded	Scored from 0 to 3 at 12 sites
Bone attrition	Scored from 0 to 3 in 14 subregions	Not scored	Not scored
Effusion	Scored from 0 to 3	Scored from 0 to 3	Scored from 0 to 3

Table 3 (Continues)

Table 3 (continued)

Comparison of Semiquantitative Scoring Systems for Knee OA

Parameter	WORMS	KOSS	BLOKS
Synovitis	Combined effusion and synovitis score	Synovial thickening scored as present or absent on sagittal T1-weighted SPGR image (location not described)	*(a)* Size of signal intensity changes in Hofffa fat pad; *(b)* 5 additional sites scored as present or absent (details of scoring not described)
Meniscal status	Anterior horn, body, and posterior horn scored separately from 0 to 4 in medial and lateral menisci: score of 1, minor radial or parrot beak tear; 2, nondisplaced tear or prior surgical repair; 3, displaced tear or partial resection; 4, complete maceration or destruction or complete resection	No subregional division of meniscus described; presence or absence of the following tears: horizontal, vertical, radial,complex, bucket handle; meniscal intrasubstance degeneration scored from 0 to 3	Anterior horn, body, and posterior horn scored separately in medial and lateral menisci; Presence or absence scored for intrameniscal signal intensity, vertical tear, horizontal tear, complex tear, root tear, macerated, meniscal cyst
Meniscal extrusion	Not scored	Scored from 0 to 3 on coronal image	Scored from 0 to 3 as medial or lateral extrusion on coronal image and as anterior extrusion for medial or lateral meniscus on sagittal image
Ligaments	Cruciate ligaments and collateral ligaments scored as intact or torn	Not scored	Cruciate ligaments scored as normal or complete tear; associated insertional BMLs scored in tibia and in femur
Periarticular features	Popliteal cysts, anserine bursitis, semimembranosus bursa, meniscal cyst, infrapatellar bursitis, prepatellar bursitis, tibiofibular cyst	Only popliteal cysts scored from 0 to 3	Patella tendon: no signal intensity change and signal intensity abnormality; the following scored as present or absent: pes anserine bursitis; Iliotibial band signal intensity; popliteal cyst; infrapatellar bursa; prepatellar bursa; ganglion cysts of the tibiofemoral joint, meniscus, anterior and posterior cruciate ligaments, semimembranosus, semitendinosus, other
Loose bodies	Scored from 0 to 3	Not scored	Scored as absent or present

Note.—BLOKS = Boston Leeds Osteoarthritis Knee Score, BML = bone marrow lesion, KOSS = Knee Osteoarthritis Scoring System, WORMS = Whole-Organ Magnetic Resonance Imaging Score.

the knee is similar to that of routine 2D and SPGR techniques (88,89). However, DEFT suffers from long acquisition times, insufficient fat saturation, and low sensitivity to bone marrow changes such as edema.

For imaging of the knee joint to investigate OA, the minimum requirement would consist of proton density– or intermediate-weighted fat-suppressed sequences in three planes plus one non–fat-suppressed T1-weighted sequence for superior visualization of bone contours, loose bodies, and subchondral sclerosis. If 3D volumetric analysis is to be included, an additional high-spatial-resolution 3D gradient-recalled-echo sequence that can provide high intrinsic cartilage signal intensity is to be included. An overview on protocol suggestions for semiquantitative assessment of knee OA was published several years ago (90).

MR Imaging Field Strength, Extremity MR Imaging, and Weight-bearing MR Imaging

Low-field-strength (0.18–0.2-T) units for imaging extremities seem outdated for morphologic assessment of knee cartilage owing to a lower signal-to-noise ratio and limitations concerning fat suppression that result in image quality inferior to that which can be achieved at 1.5 or 3 T. Although never validated against the standard of high-field-strength MR imaging, these low-field-strength techniques have been used in clinical trials for some time (91–94). However, peripheral extremity magnets have advantages: lower installation, maintenance, and management costs than large-bore magnets and greater patient comfort, especially for claustrophobic patients. In large knee OA trials, dedicated 1.0-T extremity MR imaging has demonstrated good to excellent intra- and interobserver reliability for morphologic assessment of cartilage (Fig 7) with the use of time-efficient protocols, as compared with 1.5-T imaging (46,60,95).

Imaging with a 1.5-T large-bore magnet is still regarded as the clinical standard, and most of the studies in which MR imaging is applied for morphologic and compositional assessment of knee cartilage were performed at this field strength (54,59,88,96). In recent years, 3-T systems have demonstrated promising results with regard to optimizing morphologic and compositional cartilage imaging in the knee (55,62,97). The signal-to-noise ratio is roughly twice as great at 3 T as it is at

Table 4

Characteristics, Strengths, and Drawbacks of MR Imaging Techniques for Morphologic Assessment of Knee Cartilage

MR Imaging Technique	Characteristics	Strengths	Drawbacks
2D FSE	Routine sequence for knee imaging; T1-, proton density–, and T2-weighted sequences are commonly used in both clinical and research settings	T2- and intermediate-weighted sequences provide excellent contrast between fluid and cartilage; allows assessment of other internal structures	Anisotropic voxels; section gaps; partial-volume effects
3D FSE	Uses flip-angle modulation to reduce blurring and parallel imaging time to acquire 3D FSE intermediate-weighted images	Isotropic resolution and multiplanar reformation; low potential for partial-volume artifacts; allows assessment of other internal structures	Has not yet replaced 2D FSE imaging in clinical practice; not yet applied in knee OA trials
3D SPGR	Spoils the transverse steady state by semirandomly changing the phase of the radiofrequency pulse; primarily T1- or proton density–weighted contrast	Standard for imaging of cartilage morphology; higher sensitivity than routine 2D FSE; isotropic resolution and multiplanar reformation; low potential for partial-volume artifacts	Long acquisition times; lack of contrast between fluid and cartilage; high sensitivity to susceptibility artifacts; poor for assessment of marrow abnormalities
3D DESS	Two or more gradient echoes, separated by refocusing pulse, are acquired, and both are combined to generate the image; higher T2 weighting with high signal intensity for both cartilage and fluid; higher flip angles should be considered	Faster acquisition times than SPGR; high SNR and cartilage-to-fluid contrast; isotropic resolution and multiplanar reformation; low potential for partial-volume artifacts	Intrasubstance signal intensity changes in cartilage may be difficult to detect; poor for assessment of marrow abnormalities; high sensitivity to susceptibility artifacts
3D balanced SSFP (including VIPR)	Steady-state sequence similar to DESS but with different parameters; may be combined with 3D radial k-space acquisition called VIPR-SSFP; Contrast depends on T1-to-T2 ratio (T2-weighted–toT1-weighted contrast for VIPR)	High SNR and cartilage-to-fluid contrast; useful for assessing ligaments and menisci; isotropic resolution and multiplanar reformation; low potential for partial-volume artifacts	Banding artifacts at long repetition times, especially at higher (3-T) field strength; not yet applied in knee OA trials
3D driven-equilibrium Fourier transform	Uses active return of magnetization to the z axis after each excitation, enhancing the signal intensity of fluid while preserving the that from cartilage; contrast depends on T1-to-T2 ratio	Diagnostic performance similar to that of routine 2D FSE and SPGR sequences	Long acquisition times; poor for assessment of marrow abnormalities; fat saturation is often insufficient; not yet applied in knee OA trials
3D FSE SPACE	Uses large eligible turbo factors owing to application of a restore pulse and variable flip-angle distribution (pseudo–steady state); primarily proton density–weighted contrast	May be acquired with isotropic resolution; good SNR and SNR efficiency	Long acquisition times; not yet well validated for assessment of cartilage lesions in the knee

Note.—FSE = fast spin echo, SNR = signal-to-noise ratio, SPACE = sampling perfection with application-optimized contrast using different flip-angle evolutions, SSFP = steady-state free precession, 2D = two-dimensional, VIPR = vastly interpolated projection reconstruction.

1.5 T, allowing improvement in image quality and spatial resolution, with acquisition times similar to those at 1.5 T imaging. Previous studies (98–100) have shown that imaging at 3 T allows better morphologic assessment of knee cartilage than does imaging at 1.5 T. However, the magnetic susceptibility in tissues is exacerbated, the energy deposited in the subject's tissues is higher, images are more sensitive to flow, and there is an increase in chemical shift at 3-T MR imaging, as compared with those at 1.5-T imaging.

To date, 7-T MR imaging in humans (Fig 8) has been applied only in a research setting (101–103). In the future, 7-T systems may be able to produce higher resolution images faster than 3 T systems; to date, however, the available protocols for 7-T imaging have not shown any superiority over 3-T protocols as regards knee cartilage assessment.

Vertical open MR systems that allow true static or dynamic weight-bearing imaging of the knee are available for evaluation in patients who present with internal derangements such as a tear of the anterior cruciate ligament (104). However, the field strength and image quality achievable with such magnets limits optimized assessment of cartilage. Special loading devices may also be used in conjunction with large-bore magnets; an axial compression force of approximately 50% of body weight can be applied on the knee during imaging to simulate weight-bearing. Weight-bearing MR imaging may be helpful in detecting changes in hyaline cartilage that are detectable only under loading and could be useful in detecting variations in meniscal signal intensity and extrusion (105).

Quantitative Morphologic Cartilage Assessment

Quantitative measurement of cartilage morphology exploits the 3D nature of MR imaging data for assessing tissue parameters such as volume, thickness, or

Figure 3

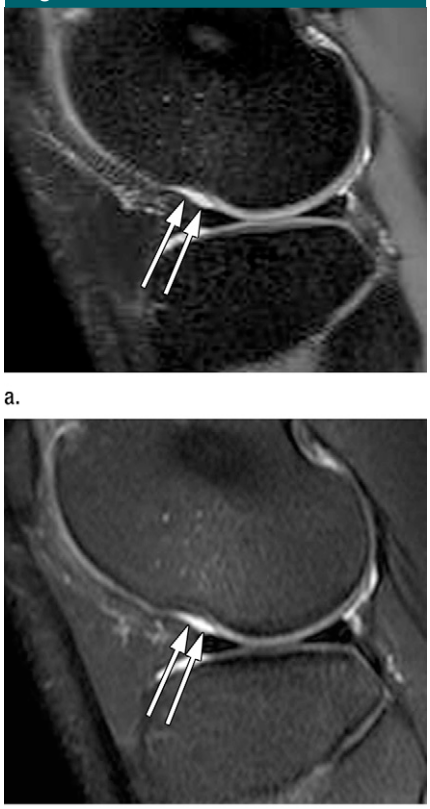

a.

b.

Figure 3: Comparison of 3D and 2D 1.5-T intermediate-weighted fat-suppressed FSE MR imaging. **(a)** Sagittal 3D image (2600/40, 0.7-mm isotropic voxels) depicts full-thickness chondral defect (arrows) accompanying osteochondral depression at the lateral femoral condyle. **(b)** Standard sagittal 2D image (3000 /48) shows defect (arrows) in similar fashion.

Figure 4

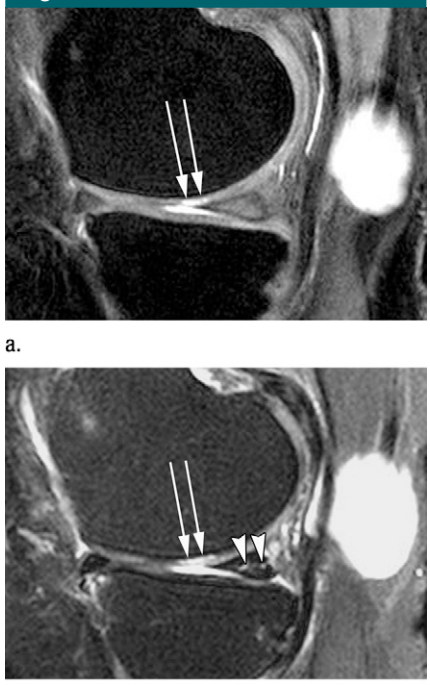

a.

b.

Figure 4: Comparison of 3-T DESS and FSE MR imaging. **(a)** Sagittal 3D water-excitation DESS image (18.2/6; flip angle, 90°) shows focal full-thickness cartilage defect (arrows) at weight-bearing medial femoral condyle. The arthrographic effect is due to excellent contrast between cartilage and synovial fluid. **(b)** Sagittal 2D T2-weighted fat-suppressed FSE image (3500/45) shows defect (arrows) in similar fashion. While **a** shows diffuse intrameniscal hyperintensity that cannot be further classified, **b** clearly depicts horizontal meniscal tear (arrowheads). Also note concomitant popliteal cyst.

Figure 5

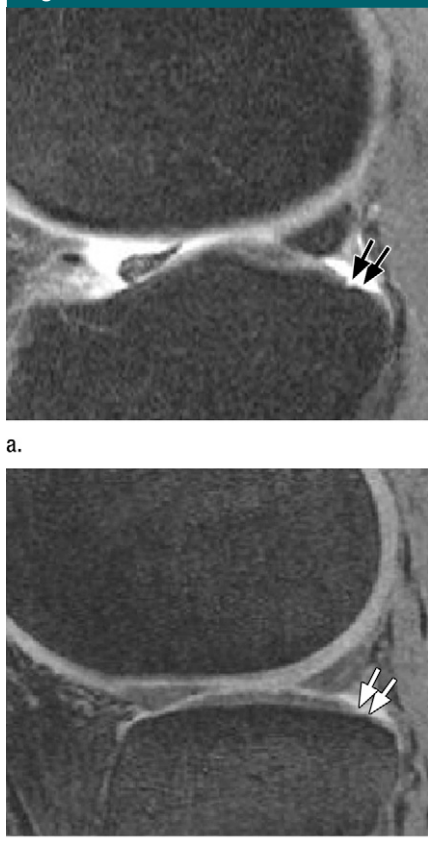

a.

b.

Figure 5: Comparison of focal defects on intermediate-weighted fat-suppressed versus DESS MR images. **(a)** Sagittal intermediate-weighted fat-suppressed image (3200/30) shows focal full-thickness cartilage defect (arrows) on posterior aspect of lateral tibial plateau. Defect is well delineated because of high contrast between intraarticular fluid and cartilage surface. **(b)** Depiction of the defect (arrows) on sagittal DESS image (16.3/4.7; flip angle, 25°) is inferior to that on **a.**

other measures as continuous variables (106). To obtain quantitative measures of cartilage morphology, the bone-cartilage interface and the cartilage surface need to be segmented by trained users, with or without assistance from segmentation software (92,107–110) (Fig 9). The disadvantage of quantitative measurement is that it requires specialized software and is very time intensive. Image analysis software can be used to compute a variety of morphologic parameters of cartilage plates, such as size of the total area of subchondral bone, area of the cartilage surface, denuded and cartilage-covered subchondral bone area, cartilage thickness over the total area of subchondral bone or cartilage-covered subchondral bone area, cartilage volume, cartilage volume normalized to cartilage thickness over the total area, and others (106,111,112).

Most investigations that deal quantitatively with cartilage morphology in OA have focused on cartilage volume, but this parameter has a number of limitations. The ability to discriminate between patients with OA and healthy subjects is limited because people with larger bones have larger cartilage volume, thus creating a wide overlap between the groups (113,114). Men have larger joint surfaces than women (and thus larger cartilage volume), even after adjustment for body height and weight (115). In longitudinal studies, the area of the subchondral bone has been shown to increase with age, both in healthy reference subjects and in patients with OA (70,116,117). These effects may mask a reduction in cartilage thickness in OA, due to the expansion of the bone and cartilage layer. Therefore, alternative outcome measures have been suggested (113,118). A novel analytic strategy for more efficient measurement of changes in cartilage thickness—independent of anatomic

Figure 6

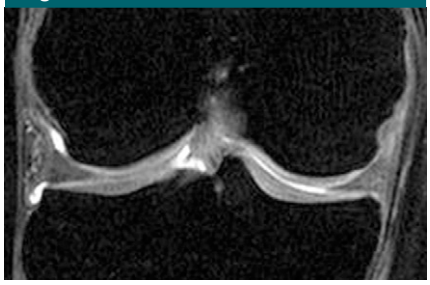

Figure 6: Coronal 3D water-excitation balanced steady-state free precession MR image (7.2/3.6) obtained at 3 T with isotropic 0.7-mm voxels mm shows excellent contrast between synovial fluid and chondral surfaces.

Figure 7

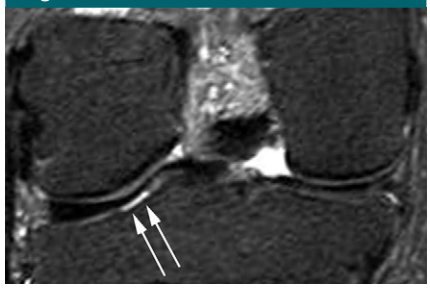

Figure 7: Extremity 1.0-T MR image. Coronal short tau inversion-recovery image (6650/15; inversion time, 100 msec) shows focal full-thickness cartilage defect at the lateral tibial plateau (arrows).

Figure 8

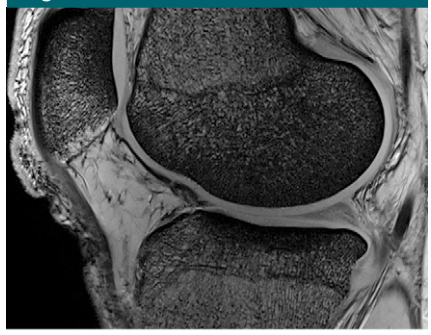

a.

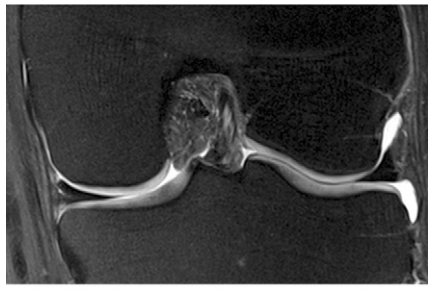

b.

Figure 8: In vivo MR imaging at very high field strength (7 T) with 28-channel knee coil. **(a)** Sagittal 3D fast low-angle shot image (20/4; resolution, 0.21 × 0.21 × 1.5 mm). **(b)** Coronal proton density–weighted fat-suppressed image (3400/25; resolution, 0.3 × 0.3 × 1.5 mm) shows excellent differentiation of articular cartilage, subchondral bone, and intraarticular joint fluid.

location—seems to result in improved discrimination between healthy subjects and patients with OA. This "ordered-values" approach also seems to be more sensitive for detecting changes longitudinally, as compared with conventional analysis, because it removes the link between magnitude and location of change and circumvents the challenge of the a priori selection of a particular knee compartment or subregion as an outcome measure of progression; thus, it might be particularly useful in the context of longitudinal clinical trials (119) (Fig 10).

The technical accuracy (validity) and test-retest precision (reproducibility) of quantitative cartilage measurements at 1.5 T have been summarized previously (69,120). Analyses based on images acquired with a dedicated 1.0-T extremity system were found to be consistent with those from 1.5-T imaging, albeit less precise (reproducible) (121). Also, quantitative cartilage measurement methods at 0.2 T have been proposed (91,92,112,122) but have not yet been validated against external standards or measurement at higher field strength.

Cartilage imaging at 3.0 T has been cross calibrated with imaging at 1.5 T, and errors of lower precision were reported for the former when thinner (1.0-mm) coronal sections were acquired with a 3-T system (123). Results of morphometric analysis from DESS images, acquired at 3 T in the Osteoarthritis Initiative, were found to be consistent with those from fast low-angle shot MR images and to display similar test-retest precision errors as fast low-angle shot images in the femorotibial joint, when both paired (124,125) and unpaired (55) reading approaches were used.

Several reports on longitudinal changes in cartilage morphology in people with OA have been published (126–138). These studies have revealed somewhat variable results in terms of the magnitude of annual cartilage loss and the sensitivity to change (mean change divided by the standard deviation of change), as summarized previously (69,120). Authors of two studies reported almost no loss in cartilage volume during a 1-year (137) and a 3-year period (130), whereas authors of other studies reported up to a 7% annual loss in the tibiofemoral cartilage plates (132). Reasons for these variations may include variability in imaging and image analysis technology, differences in risk factor profiles between cohorts, differences in study duration, experience and blinding of the readers, among others.

After anterior cruciate ligament rupture, reductions in cartilage volume and thickness were observed in the femoral trochlea, whereas increases in cartilage volume and thickness were found in the weight-bearing medial femur (139). The latter observation may be consistent with cartilage swelling or hypertrophy, which has been observed as a sign of early OA in animal models (140–143).

Risk factors for cartilage loss, as identified with quantitative measurement of cartilage morphology, include a high body mass index (126,129,133,138,144), meniscal extrusion and meniscal tears (134,135,145), knee malalignment (114, 127,145,146), advanced radiographic OA (126,129,138), bone marrow alterations (129,147,148), focal cartilage lesions (149,150), and smoking (151,152).

MR Imaging of Biochemical Properties of Articular Cartilage

OA changes in hyaline articular cartilage are characterized by important changes in the biochemical composition of cartilage. The macromolecular network of cartilage consists mainly of collagen and proteoglycans. Normally, the collagen network is highly organized, serves as the tissue's structural framework, and is the principal source of tensile and shear strength. Glucosaminoglycans (GAGs) are repeating disaccharides with

Figure 9

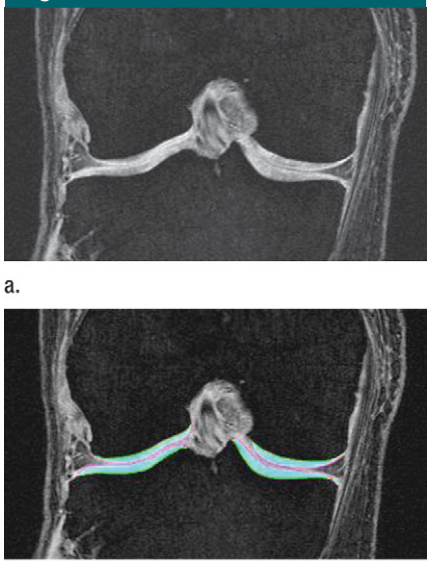

a.

b.

Figure 9: Coronal fast low-angle shot MR images (20/7.6; flip angle, 12°) demonstrate 3D morphometry. **(a)** Articular cartilage has high intensity signal and high contrast between subchondral bone and cartilage. **(b)** After manual segmentation, cartilage is outlined and color-coded in turquoise. (Courtesy of Felix Eckstein, MD, Paracelsus Medical University, Salzburg, Austria.)

Figure 10

Figure 10: Subregional division of the articular surfaces, which has gained increasing importance recently owing to analytic methods that use ordered values of subregions as outcomes. **(a)** En face view of articular surfaces of medial (right) and lateral (left) tibia. Subregions are color coded: Light blue = anterior medial-lateral tibia, red = central medial-lateral tibia, dark green = external medial-lateral tibia, dark blue = internal medial-lateral tibia, light green = posterior medial-lateral tibia. **(b)** Lateral view of the color-coded lateral femoral (top) and tibial (bottom) surfaces. (Courtesy of Felix Eckstein, MD, Paracelsus Medical University, Salzburg, Austria.)

carboxyl and sulfate groups attached to the larger aggrecan molecule that is part of the extracellular matrix network of cartilage. GAG molecules possess considerable net negative charge and confer compressive strength to the cartilage. Loss of GAGs and increased water content represent the earliest stage of cartilage degeneration, while the collagenous component of the extracellular matrix still remains intact. Several MR imaging techniques are available that enable detection of biochemical changes that precede the morphologic degeneration in cartilage. All of these techniques attempt to selectively demonstrate the GAG components and/or the collagen fiber network of the extracellular matrix and are usually summarized as "compositional imaging" of cartilage (Fig 11). An overview of the different techniques of compositional MR imaging of cartilage is presented in Table 5.

The dGEMRIC and sodium 23 (^{23}Na) MR imaging techniques are based on similar principles, with positive sodium ions being attracted by the negative fixed charged density of the GAG side chains. These electrostatic forces are responsible for a direct relationship between the local sodium concentration and fixed charged density with a strong correlation between fixed charged density and GAG content (153,154). dGEMRIC is based on the fact that GAGs contain negatively charged side chains, which lead to an inverse distribution of negatively charged contrast agent molecules (eg, gadolinium) with respect to GAG concentration (155,156) (Fig 11b). Drawbacks of this technique are the need to use a double dose of a gadolinium-based contrast agent (0.2 mmol per kilogram of body weight) and the requirement for a delay between intravenous administration of the agent and the start of the MR examination (usually 60–90 minutes) to allow complete penetration of the contrast agent into the cartilage.

Varus malalignment is associated with a lower dGEMRIC index on the medial side, while the opposite trend is evident in valgus malalignment (157). Correlations between dGEMRIC index and pain, as measured by the Western Ontario and McMaster Universities Arthritis Index, were evident in patients with hip dysplasia (157). dGEMRIC studies have demonstrated that moderate exercise can improve knee cartilage GAG (estimated by T1 in the presence of gadopentetate dimeglumine) in patients at high risk for OA (158). In patients with an injury to the anterior cruciate ligament, lower GAG concentrations were found in the medial compartment of the femoral and tibial articular cartilage of the injured knee when compared with the contralateral (uninjured) knee (159). In patients with femoroacetabular impingement, correlations were observed between dGEMRIC index, pain, and α angle, suggesting that hips with more femoral deformity may show signs of early OA (160).

T1ρ is a time constant that characterizes magnetic relaxation of spins under the influence of a radiofrequency field parallel to the spin magnetization. The resultant contrast is sensitive to the low-frequency interactions between water molecules and their local macromolecular environment, such as GAG and collagen, which are the main constituents of the extracellular matrix in cartilage. In early studies, changes in T1ρ were found in proteoglycan-depleted cartilage plugs, but, on the other hand, other investigators (161–166) reported that T1ρ did not correspond to a modified dGEMRIC technique or to the proteoglycan distribution seen at histologic examination, which suggests that several factors contribute to variations in T1ρ. Recently, rapid 3D in vivo T1ρ mapping techniques of knee cartilage at high field strength (3 T) have been developed and applied in patients with OA (167–170). Other in vivo studies (164,171) have shown increased cartilage T1ρ values in patients with OA

Figure 11

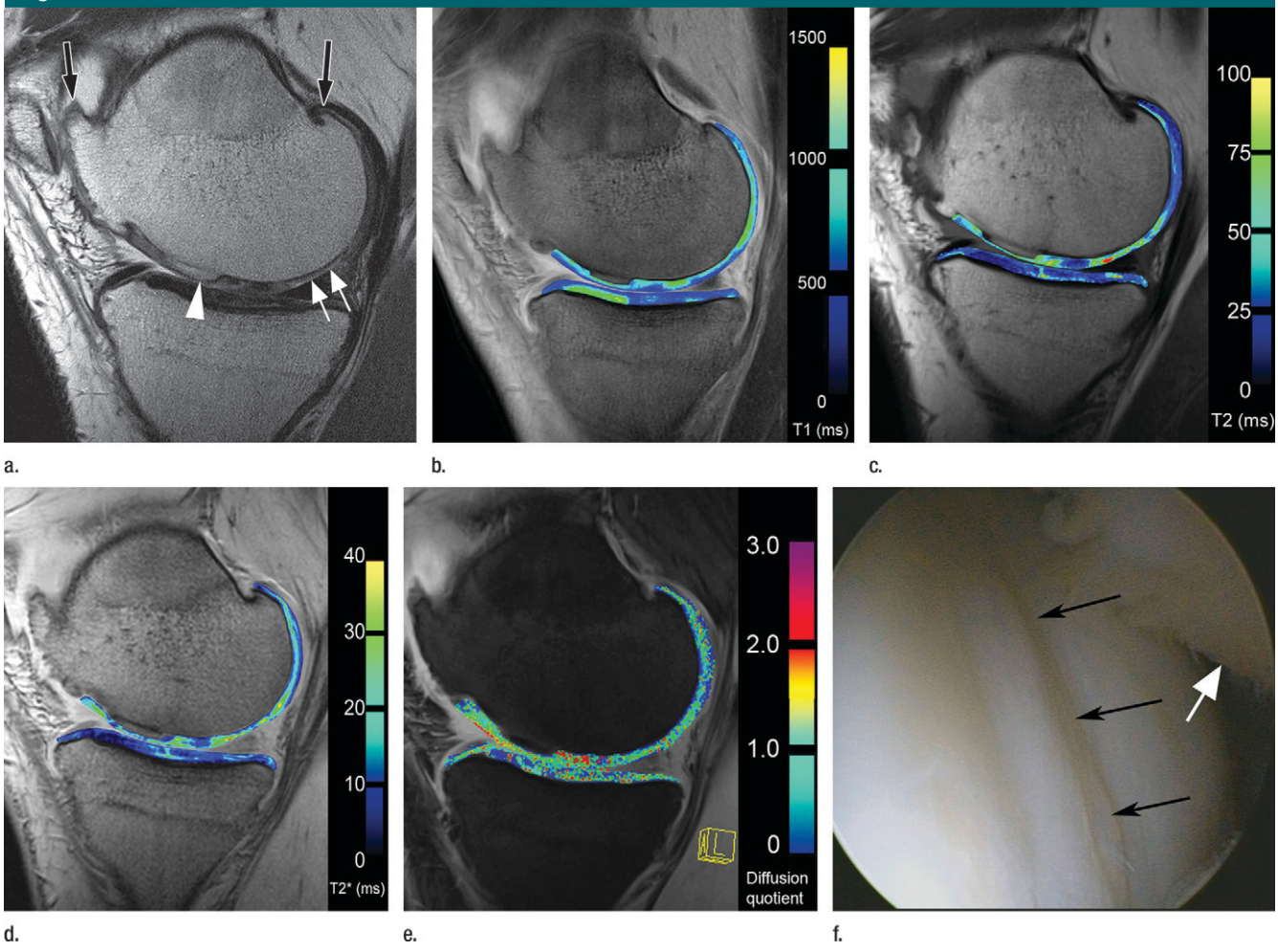

Figure 11: Compositional MR imaging. **(a)** Sagittal proton density–weighted high-spatial-resolution 3-T MR image (3200/35) of medial compartment of a knee with tibiofemoral OA shows peripheral (black arrows) and central (arrowhead) osteophytes. Focal cartilage thinning is shown in the medial femoral condyle adjacent to the posterior horn of the medial meniscus (white arrows) and in posterior part of the tibial plateau. **(b)** Delayed gadolinium-enhanced MR imaging of cartilage (dGEMRIC) T1 map (490/13) corresponding to **a** shows multiple areas with low T1 values, corresponding to low GAG content in superficial layers of femoral cartilage and in posterior part of tibial cartilage (dark blue). **(c)** Sagittal T2 map (2700/10–70; flip angle, 180°) corresponding to **a** reveals several areas of increased T2 values in femoral medial condyle and largely corresponding to **b**. Dark blue = low T2 values, light blue and yellow = higher T2 values. In contrast, only minimal abnormalities in T2 values are seen in tibial cartilage. **(d)** Sagittal T2* map (177/5.7–26.4; flip angle, 35°) corresponding to **a** shows comparable abnormalities as those in **c. (e)** Corresponding sagittal diffusion-weighted MR image (16.3/5.9; flip angle, 30°) shows minor restrictions in diffusion in central region of femoral condyle cartilage and in central and posterior portions of tibial cartilage layer (red). **(f)** Corresponding arthroscopic image verifies femoral cartilage damage (black arrows). White arrow = posterior horn of medial meniscus. (Fig 11f courtesy of Department of Orthopedics, University of Vienna, Austria.)

compared with those values in control subjects, which suggests the potential for T1ρ imaging for noninvasive evaluation of diseased cartilage. In cartilage overlying traumatic bone marrow lesions, the average T1ρ values were significantly higher than those in surrounding cartilage, demonstrating that macromolecular changes in cartilage may be related to traumatic bone marrow damage (172).

Previous research (153,173,174) has already shown that ^{23}Na MR imaging has a potential advantage over conventional proton MR imaging for the investigation of biochemical markers in cartilage during the early stages of OA. Although ^{23}Na MR imaging has high specificity and does not require any exogenous contrast agent, it does require special hardware (multinuclear) capabilities, specialized RF coils (transmit-receive coils), and, likely, 3D very short echo time sequences. These challenges currently limit the use of ^{23}Na MR imaging in the clinical and research settings.

T2 mapping has been used to describe the composition of hyaline articular cartilage in the knee joint on the basis of collagen structure and hydration (175) (Fig 11c). In addition to the transverse relaxation time (T2) of articular

Table 5

Characteristics, Strengths, and Drawbacks of Compositional MR Imaging for Assessment of Knee Cartilage

Type of MR Examination	Cartilage Component	Strengths	Drawbacks
dGEMRIC	GAG specific	Correlates indirectly with GAG, clinically useful and validated technique	Requires intravenous contrast agent and delay between contrast agent administration and MR examination
Sodium 23 MR imaging	GAG specific	Correlates directly with GAG, no contrast agent needed	Technically demanding, requires very high field strength multinuclear capable system and resonance-specific coils
T2 mapping	Collagen network and water-content specific	Clinically useful, validated, robust technique	2D technique, time consuming
T2* mapping	Collagen network and content specific	3D isotropic capability, short examination time	Collagen specificity not well defined
T1ρ mapping	Collagen network and GAG specific	Robust technique	Specific absorption rate problems, specificity for cartilage components is unclear
Diffusion-weighted MR imaging	Collagen network and GAG specific	Provides information in addition to GAG and collagen specificity	Sensitive to motion artifacts, absolute quantification can be demanding in thin cartilage layers

cartilage, T2* relaxation measures have recently been investigated (154) for depiction of the collagen matrix (Fig 11d). In healthy articular cartilage, an increase in T2 values from deep to superficial cartilage layers can be observed; this is based on the anisotropy of collagen fibers running perpendicular to cortical bone in the deep layer of cartilage (176). Therefore, zonal evaluation of articular cartilage is important in T2 analyses. Analyses of T2 relaxation times in the knee have been performed previously (177,178), usually at 1.5 T or, more recently, 3.0 T, demonstrating the ability to depict abnormalities before there is evident morphologic change. In vivo MR imaging studies (179) have demonstrated that cartilage T2 values are related to age and vary from the subchondral bone to the cartilage surface. Cartilage T2 values seem to be associated with the severity of OA, and there are variations between tibial and femoral cartilage T2 (180). A significant correlation between patellar cartilage T2 and the severity and grade of cartilage and meniscus lesions has been demonstrated. Subjects with high activity levels had significantly higher prevalence and grade of abnormalities and higher T2 values than did subjects with low activity levels (181).

Evaluation of Cartilage Repair

Surgical approaches to repair focal cartilage damage were introduced several years ago and have shown promising results, albeit long-term observation of any of the repair techniques still have not been reported (182,183). The most commonly applied techniques are microfracture, osteochondral transfer, and autologous chondrocyte implantation (184,185) (Fig 12).

Microfracture has been shown to be an efficient one-step procedure, but it produces mainly fibrous repair tissue with incomplete filling of the defect and limited load-bearing capacity. In osteochondral graft transplantation, osteochondral plugs are taken from non–weight-bearing areas in the femoral condyles or areas that less frequently bear weight. A cylindric cutting device is used, and the plugs are implanted as a mosaic to fill the defect(s) (182). Autologous chondrocyte implantation is a two-step procedure, with sampling of cartilage, in vitro cultivation of 4–6 weeks, and reimplantation. During reimplantation, chondrocytes are applied to the damaged area in combination with a membrane (either a periosteal flap or a collagen membrane in standard autologous chondrocyte implantation) or are preseeded in a scaffold matrix (in matrix-associated chondrocyte implantation).

A description of the repair tissue may be based on morphologic semiquantitative or compositional approaches (185–189). Perhaps the most comprehensive semiquantitative MR imaging evaluation is performed with the magnetic resonance observation of cartilage repair tissue (MOCART) scoring system (188,189). The validity and reliability of this system has been evaluated with nine pertinent variables. These include filling of the defect, integration of the border zone to the adjacent cartilage, intactness of the subchondral lamina, intactness of the subchondral bone, signal intensity of the repair tissue relative to that of adjacent native cartilage, and others. The normal and abnormal morphologic appearances of cartilage have been described in detail elsewhere (185,186). MOCART has been applied to all cartilage repair procedures in a longitudinal fashion by using 2D and 3D MR imaging techniques (190–193).

dGEMRIC has been used to evaluate relative GAG content of repair tissue in patients who have undergone different surgical cartilage repair techniques (194,195) (Fig 12b). Whereas in some studies, the GAG concentration in repair

Figure 12

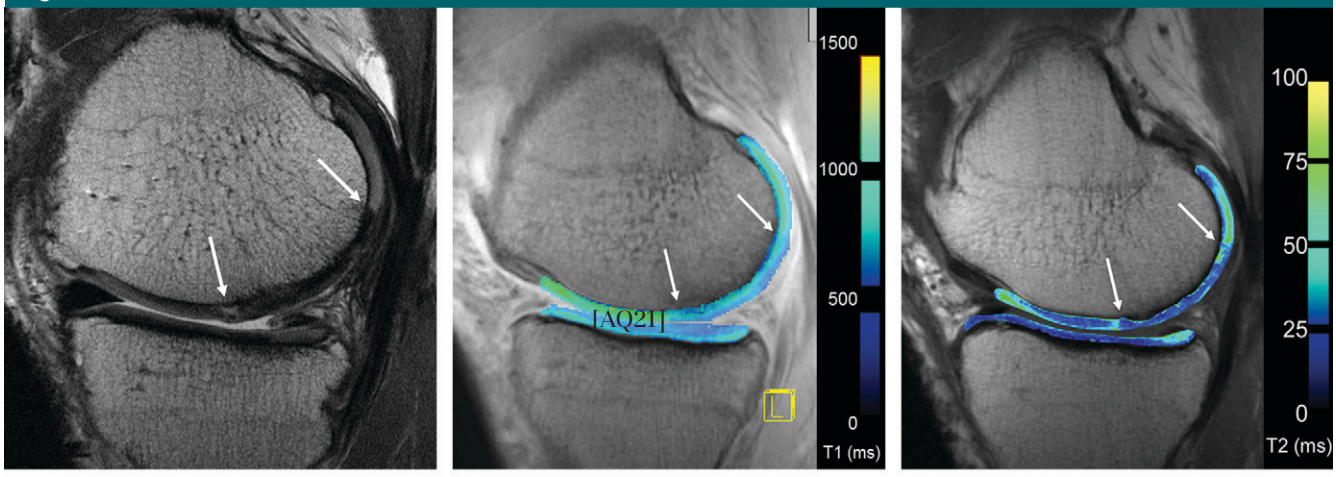

Figure 12: Sagittal MR images of cartilage repair. Arrows = anterior and posterior margins of transplant. **(a)** Proton density–weighted high-spatial-resolution image (3200/30) of medial tibiofemoral compartment 4 years after matrix-associated fibrin-gel–based autologous chondrocyte transplantation. Complete filling of femoral cartilage defect with complete peripheral and central integration to adjacent cartilage and subchondral bone. Surface of the transplant is smooth and the structure is homogeneous. Signal intensity is markedly lower than that of normal hyaline cartilage. **(b)** Corresponding contrast-enhanced T1 map (dGEMRIC, 490/13) shows homogeneously lower T1 values in cartilage transplant, as compared with normal hyaline cartilage (blue). **(c)** Corresponding T2 map (2700/10–70; flip angle, 180°) shows comparable T2 values in cartilage transplant region, as compared with those of normal hyaline cartilage.

cartilage 10 months (or longer) after autologous chondrocyte implantation was comparable to the GAG concentration in adjacent normal hyaline cartilage, in other studies a significantly lower GAG content in repair tissue more than 1 year after surgery has been reported (196,197). Histologic correlation has shown that patients with matrix-associated autologous chondrocyte implantation may show different types of repair tissue, from hyaline-like to mixed hyaline-fibrous and fibrous tissue over time, which may partly explain these discrepant findings (198,199). In one of these studies (97), 20 age-matched patients treated with either microfracture or autologous chondrocyte implantation were evaluated after a comparable postoperative interval, and the microfracture-treated knees had lower GAG content. As is known from histologic studies (200,201), repair tissue formed by microfracture contains fewer proteoglycans and an abnormal distribution of collagen than does normal cartilage.

T2 mapping has been used for quantitative comparison of repair tissue and normal hyaline cartilage. Domayer et al (191) described a T2 index, defined by the mean global T2 in repair tissue divided by the mean global T2 in normal cartilage times 100; this T2 index correlated with clinical outcome measures. In a study by Welsch et al (202), mean T2 was significantly reduced following microfracturing but not for matrix-associated autologous chondrocyte implantation. The repair tissue after microfracturing showed no significant depth-related variation, whereas matrix-associated autologous chondrocyte implantation showed a significant increase from the deep to the superficial zone, as seen in intact hyaline cartilage (202). Zonal assessment of repair tissue is paramount, as this will help to discern differences between disorganized repair tissue and the stratified T2 values of intact hyaline cartilage. Reported prolonged T2 values from the condyle, compared with values obtained from the patella repair tissue, indicate differential maturation of the repair tissue as a function of its environment (186).

Studies of diffusion-weighted MR imaging have focused on the steady-state free precession sequence, which is based on a reversed fast imaging with steady-state precession approach and provides a semiquantitative assessment of diffusion in hyaline cartilage and cartilage repair tissue (187,203,204). In a longitudinal study on autologous chondrocyte implantation, the diffusivity of repair tissue decreased over time toward the values in healthy control cartilage (203). In a multimodal approach, repair tissue after microfracture and autologous chondrocyte implantation were compared, and the diffusivity of the repair tissue after microfracture appeared to be higher than that after autologous chondrocyte implantation; an initial correlation with clinical results could be shown (187,205). Recently developed steady-state free precession diffusion-weighted imaging sequences provide direct quantification with the apparent diffusion coefficient, which, for future diffusion-weighted imaging approaches, will add important information to the evaluation of cartilage repair procedures.

The Role of US

Although the application of US in inflammatory diseases is common and widespread, it has been applied to OA less frequently. A comprehensive overview of the topic was recently presented by Keen et al (206). US allows sensitive

and specific identification of soft-tissue and bone changes, with the advantage of noninvasive assessment of vascularity (207). In contrast to radiography, US does not use ionizing radiation, can image the joint in multiple planes, and allows dynamic assessment of moving structures (208). However, acquisition of US skills takes time and practice and ongoing maintenance of competency (209). The main limitation of US is its inability to depict much beyond bone interfaces or into deeper articular structures. However, US is able to depict the patellofemoral joint (including the anterior femoral surface and the Hoffa fat pad) and the medial and lateral joint line (including osteophytes and the body of the meniscus). Furthermore, periarticular cystic lesions are well depicted.

US has proved to be a useful adjuvant modality, rather than a standalone diagnostic test, for routine clinical assessment to aid management of disease (210). For research purposes, universally applicable scoring systems are needed that show good reliability and demonstrable sensitivity to change. The benefits of US over radiography include the ability to image soft-tissue structures and the potential to detect small or early structural lesions (211,212). Whether there will be a role for US in the assessment of OA before it becomes radiographically visible remains to be seen.

Treatment

The aims of any treatment strategy for OA are *(a)* patient education about the disease, *(b)* pain control, *(c)* improved function and decreased disability, and *(d)* potential alteration of the disease process and its consequences (213).

In the absence of a cure, the present therapeutic approaches primarily attempt to alleviate pain and improve joint function. Treatment plans should never be defined according to the radiographic appearance of the joint but should be individualized according to the clinical symptoms and the specific findings of the clinical examination, taking into account concomitant obesity, malalignment, and muscle weakness. The recommended hierarchy of treatment should consist of nonpharmacologic options first, followed by drugs and, ultimately, surgery. The typical indications for surgery are debilitating pain and major limitation of functions such as walking, working, or sleeping. If surgical intervention is to be pursued, recent evidence has shown that patients who undergo surgery in a low-volume hospital or by a low-volume surgeon have worse functional outcome than do those treated in a high-volume hospital or by a high-volume surgeon (214).

The American College of Rheumatology expert-guided consensus guidelines for the management of hip and knee OA published in 2000 (215) seem somewhat outdated, but are currently undergoing revision. Treatment guidelines and recommendations by the Osteoarthritis Research Society International and the European League against Rheumatism should be used instead as a guide to any individualized treatment approach. These also cover more recent knowledge on the use of hyaluronate, chondroitin and glucosamine (216,217).

Outlook

OA is still considered an enigmatic pathologic condition, with only symptomatic treatment available and limited therapeutic options to modify structural disease. Publicly available Osteoarthritis Initiative MR imaging data, together with data from other ongoing large epidemiologic studies, will provide ample opportunity for collaborative research into all aspects of imaging in OA and should allow the research community to rapidly advance its understanding of the risk factors involved in OA disease progression. These will also help in the development of successful strategies for disease prevention. Most important, imaging data will enable us to determine which imaging biomarkers are the best predictors of clinical outcomes, such as real or virtual total joint replacement. These data sets will further help in the validation of new imaging biomarkers as surrogate measures of disease progression, particularly in therapeutic intervention trials and, eventually, in clinical management. Further improvements in imaging hardware, coils, sequences, and image analysis algorithms may foster a more comprehensive understanding of cartilage morphology and composition and of other articular tissues than is currently possible. The use of high-spatial-resolution techniques to assess cartilage morphology, combined with available compositional techniques, will improve the sensitivity of MR imaging for the detection of early cartilaginous degeneration, as well as the ability of MR imaging to help assess different cartilage repair techniques, which most probably will strengthen the role of imaging in the clinical setting in the future.

This will be of particular importance once structure- or disease-modifying drugs become available, which will require monitoring of the treatment response in large sets of OA patients. With the availability of disease-modifying interventions, imaging will play an important and meaningful role in clinical decision making and practice.

Acknowledgments: We acknowledge the valuable input of the following experts in the field who contributed greatly to shape this review: Garry Gold, MD, Felix Eckstein, MD, Marie-Pierre Hellio Le Graverand, MD, PhD, DSc, Goetz Welsch, MD, Philip Conaghan, MBBS, PhD, FRACP, FRCP, and Helen Keen, MBBS, FRACP.

Disclosures of Potential Conflicts of Interest: F.W.R. Financial activities related to the present article: none to disclose. Financial activities not related to the present article: is a shareholder in and vice-president of Boston Imaging Core Lab (BICL). Other relationships: none to disclose. **M.D.C.** Financial activities related to the present article: none to disclose. Financial activities not related to the present article: is a shareholder in BICL. Other relationships: none to disclose. **S.T.** Financial activities related to the present article: none to disclose. Financial activities not related to the present article: none to disclose. Other relationships: none to disclose. **A.G.** Financial activities related to the present article: none to disclose. Financial activities not related to the present article: is president of BICL; served as consultant to and received speaking fees and/or honoraria from Facet Solutions, Genzyme, Stryker, and Merck Serono; has a research grant from GE Healthcare. Other relationships: none to disclose.

References

1. Lawrence RC, Helmick CG, Arnett FC, et al. Estimates of the prevalence of arthritis and selected musculoskeletal disorders in the United States. Arthritis Rheum 1998;41(5):778–799.

2. Centers for Disease Control and Prevention (CDC). Prevalence of disabilities and associated health conditions among adults—United States, 1999. MMWR Morb Mortal Wkly Rep 2001;50(7):120–125.

3. Lawrence RC, Felson DT, Helmick CG, et al. Estimates of the prevalence of arthritis and other rheumatic conditions in the United States. Part II. Arthritis Rheum 2008;58(1):26–35.

4. Centers for Disease Control and Prevention (CDC). Arthritis prevalence and activity limitations—United States, 1990. MMWR Morb Mortal Wkly Rep 1994;43(24):433–438.

5. Helmick CG, Felson DT, Lawrence RC, et al. Estimates of the prevalence of arthritis and other rheumatic conditions in the United States. Part I. Arthritis Rheum 2008;58(1):15–25.

6. Nuki G. Osteoarthritis: a problem of joint failure. Z Rheumatol 1999;58(3):142–147.

7. Eyre DR. Collagens and cartilage matrix homeostasis. Clin Orthop Relat Res 2004;(427 Suppl):S118–S122.

8. Aigner N, Van der Kraan P, Van den Berg W. Osteoarthritis and inflammation: inflammatory changes in osteoarthritis synoviopathy. In: Buckwalter J, Lotz M, Stoltz JF, eds. Osteoarthritis, inflammation and degradation: a continuum. Amsterdam, the Netherlands: IOS, 2007; 219–235.

9. Valdes AM, Loughlin J, Oene MV, et al. Sex and ethnic differences in the association of ASPN, CALM1, COL2A1, COMP, and FRZB with genetic susceptibility to osteoarthritis of the knee. Arthritis Rheum 2007;56(1):137–146.

10. Kornaat PR, Sharma R, van der Geest RJ, et al. Positive association between increased popliteal artery vessel wall thickness and generalized osteoarthritis: is OA also part of the metabolic syndrome? Skeletal Radiol 2009;38(12):1147–1151.

11. Hunter DJ. Risk stratification for knee osteoarthritis progression: a narrative review. Osteoarthritis Cartilage 2009;17(11):1402–1407.

12. Hellio Le Graverand-Gastineau MP. OA clinical trials: current targets and trials for OA. Choosing molecular targets: what have we learned and where we are headed? Osteoarthritis Cartilage 2009;17(11):1393–1401.

13. Altman R, Asch E, Bloch D, et al. Development of criteria for the classification and reporting of osteoarthritis. Classification of osteoarthritis of the knee. Diagnostic and Therapeutic Criteria Committee of the American Rheumatism Association. Arthritis Rheum 1986;29(8):1039–1049.

14. Spector TD, Hart DJ, Byrne J, Harris PA, Dacre JE, Doyle DV. Definition of osteoarthritis of the knee for epidemiological studies. Ann Rheum Dis 1993;52(11):790–794.

15. Kellgren JH, Lawrence JS. Radiological assessment of osteo-arthrosis. Ann Rheum Dis 1957;16(4):494–502.

16. Altman RD, Hochberg M, Murphy WA Jr, Wolfe F, Lequesne M. Atlas of individual radiographic features in osteoarthritis. Osteoarthritis Cartilage 1995;3(Suppl A):3–70.

17. Scott WW Jr, Lethbridge-Cejku M, Reichle R, Wigley FM, Tobin JD, Hochberg MC. Reliability of grading scales for individual radiographic features of osteoarthritis of the knee. The Baltimore longitudinal study of aging atlas of knee osteoarthritis. Invest Radiol 1993;28(6):497–501.

18. Altman RD, Gold GE. Atlas of individual radiographic features in osteoarthritis, revised. Osteoarthritis Cartilage 2007;15(Suppl A):A1–A56.

19. Bauer DC, Hunter DJ, Abramson SB, et al. Classification of osteoarthritis biomarkers: a proposed approach. Osteoarthritis Cartilage 2006;14(8):723–727.

20. Amin S, LaValley MP, Guermazi A, et al. The relationship between cartilage loss on magnetic resonance imaging and radiographic progression in men and women with knee osteoarthritis. Arthritis Rheum 2005;52(10):3152–3159.

21. Leach RE, Gregg T, Siber FJ. Weight-bearing radiography in osteoarthritis of the knee. Radiology 1970;97(2):265–268.

22. Mazzuca SA, Brandt KD, Katz BP. Is conventional radiography suitable for evaluation of a disease-modifying drug in patients with knee osteoarthritis? Osteoarthritis Cartilage 1997;5(4):217–226.

23. Messieh SS, Fowler PJ, Munro T. Anteroposterior radiographs of the osteoarthritic knee. J Bone Joint Surg Br 1990;72(4):639–640.

24. Buckland-Wright JC, Wolfe F, Ward RJ, Flowers N, Hayne C. Substantial superiority of semiflexed (MTP) views in knee osteoarthritis: a comparative radiographic study, without fluoroscopy, of standing extended, semiflexed (MTP), and schuss views. J Rheumatol 1999;26(12):2664–2674.

25. Peterfy C, Li J, Zaim S, et al. Comparison of fixed-flexion positioning with fluoroscopic semi-flexed positioning for quantifying radiographic joint-space width in the knee: test-retest reproducibility. Skeletal Radiol 2003;32(3):128–132.

26. Buckland-Wright JC, Macfarlane DG, Williams SA, Ward RJ. Accuracy and precision of joint space width measurements in standard and macroradiographs of osteoarthritic knees. Ann Rheum Dis 1995;54(11):872–880.

27. Mazzuca SA, Brandt KD, Buckland-Wright JC, et al. Field test of the reproducibility of automated measurements of medial tibiofemoral joint space width derived from standardized knee radiographs. J Rheumatol 1999;26(6):1359–1365.

28. Lequesne M. Chondrometry. Quantitative evaluation of joint space width and rate of joint space loss in osteoarthritis of the hip. Rev Rhum Engl Ed 1995;62(3):155–158.

29. Ravaud P, Chastang C, Auleley GR, et al. Assessment of joint space width in patients with osteoarthritis of the knee: a comparison of 4 measuring instruments. J Rheumatol 1996;23(10):1749–1755.

30. Cootes TF, Taylor CJ. Anatomical statistical models and their role in feature extraction. Br J Radiol 2004;77(Spec No 2):S133–S139.

31. Seise M, McKenna SJ, Ricketts IW, Wigderowitz CA. Learning active shape models for bifurcating contours. IEEE Trans Med Imaging 2007;26(5):666–677.

32. Conrozier T, Lequesne M, Favret H, et al. Measurement of the radiological hip joint space width. An evaluation of various methods of measurement. Osteoarthritis Cartilage 2001;9(3):281–286.

33. Vignon E. Radiographic issues in imaging the progression of hip and knee osteoarthritis. J Rheumatol Suppl 2004;70:36–44.

34. Duryea J, Zaim S, Genant HK. New radiographic-based surrogate outcome measures for osteoarthritis of the knee. Osteoarthritis Cartilage 2003;11(2):102–110.

35. Neumann G, Hunter DJ, Nevitt MC, et al. Location specific radiographic joint space width for osteoarthritis progression. Osteoarthritis Cartilage 2009;17(6):761–765.

36. Bruyère O, Henrotin YE, Honoré A, et al. Impact of the joint space width measurement method on the design of knee osteoarthritis studies. Aging Clin Exp Res 2003;15(2):136–141.

37. Mazzuca SA, Brandt KD, Lane KA, Katz BP. Knee pain reduces joint space width in conventional standing anteroposterior radiographs of osteoarthritic knees. Arthritis Rheum 2002;46(5):1223–1227.

38. Peterfy CG, White D. Whole-organ evaluation of the knee in osteoarthritis using MRI [abstr]. Ann Rheum Dis 1999;38:342.

39. Hunter DJ, Zhang YQ, Niu JB, et al. The association of meniscal pathologic changes with cartilage loss in symptomatic knee osteoarthritis. Arthritis Rheum 2006;54(3):795–801.

40. Englund M, Guermazi A, Roemer FW, et al. Meniscal tear in knees without surgery and the development of radiographic osteoarthritis among middle-aged and elderly persons: The Multicenter Osteoarthritis Study. Arthritis Rheum 2009;60(3):831–839.

41. Englund M, Guermazi A, Roemer FW, et al. Meniscal pathology on MRI increases the risk for both incident and enlarging subchondral bone marrow lesions of the knee: the MOST Study. Ann Rheum Dis 2010; 69(10):1796–1802.

42. Hernández-Molina G, Neogi T, Hunter DJ, et al. The association of bone attrition with knee pain and other MRI features of osteoarthritis. Ann Rheum Dis 2008;67(1):43–47.

43. Felson DT, McLaughlin S, Goggins J, et al. Bone marrow edema and its relation to progression of knee osteoarthritis. Ann Intern Med 2003;139(5 Pt 1):330–336.

44. Felson DT, Niu J, Guermazi A, et al. Correlation of the development of knee pain with enlarging bone marrow lesions on magnetic resonance imaging. Arthritis Rheum 2007; 56(9):2986–2992.

45. Reichenbach S, Yang M, Eckstein F, et al. Does cartilage volume or thickness distinguish knees with and without mild radiographic osteoarthritis? The Framingham Study. Ann Rheum Dis 2010;69(1):143–149.

46. Roemer FW, Zhang Y, Niu J, et al. Tibiofemoral joint osteoarthritis: risk factors for MR-depicted fast cartilage loss over a 30-month period in the multicenter osteoarthritis study. Radiology 2009;252(3):772–780.

47. Neogi T, Nevitt M, Niu J, et al. Subchondral bone attrition may be a reflection of compartment-specific mechanical load: the MOST Study. Ann Rheum Dis 2010;69(5):841–844.

48. Roemer FW, Guermazi A, Javaid MK, et al. Change in MRI-detected subchondral bone marrow lesions is associated with cartilage loss: the MOST Study. A longitudinal multicentre study of knee osteoarthritis. Ann Rheum Dis 2009;68(9):1461–1465.

49. Hunter DJ, Lo GH, Gale D, Grainger AJ, Guermazi A, Conaghan PG. The reliability of a new scoring system for knee osteoarthritis MRI and the validity of bone marrow lesion assessment: BLOKS (Boston Leeds Osteoarthritis Knee Score). Ann Rheum Dis 2008;67(2):206–211.

50. Kornaat PR, Ceulemans RY, Kroon HM, et al. MRI assessment of knee osteoarthritis: Knee Osteoarthritis Scoring System (KOSS)—inter-observer and intra-observer reproducibility of a compartment-based scoring system. Skeletal Radiol 2005;34(2):95–102.

51. Peterfy CG, Guermazi A, Zaim S, et al. Whole-Organ Magnetic Resonance Imaging Score (WORMS) of the knee in osteoarthritis. Osteoarthritis Cartilage 2004;12(3):177–190.

52. Hernández-Molina G, Guermazi A, Niu J, et al. Central bone marrow lesions in symptomatic knee osteoarthritis and their relationship to anterior cruciate ligament tears and cartilage loss. Arthritis Rheum 2008; 58(1):130–136.

53. Guermazi A, Roemer FW, Hayashi D, et al. Extended report: assessment of synovitis with contrast-enhanced MRI using a whole-joint semiquantitative scoring system in people with, or at high risk of, knee osteoarthritis—the MOST study. Ann Rheum Dis 2011;70(5):805–811.

54. Duc SR, Pfirrmann CW, Schmid MR, et al. Articular cartilage defects detected with 3D water-excitation true FISP: prospective comparison with sequences commonly used for knee imaging. Radiology 2007;245(1):216–223.

55. Eckstein F, Hudelmaier M, Wirth W, et al. Double echo steady state magnetic resonance imaging of knee articular cartilage at 3 Tesla: a pilot study for the Osteoarthritis Initiative. Ann Rheum Dis 2006;65(4):433–441.

56. Mohr A. The value of water-excitation 3D FLASH and fat-saturated PDw TSE MR imaging for detecting and grading articular cartilage lesions of the knee. Skeletal Radiol 2003;32(7):396–402.

57. Mohr A, Priebe M, Taouli B, Grimm J, Heller M, Brossmann J. Selective water excitation for faster MR imaging of articular cartilage defects: initial clinical results. Eur Radiol 2003;13(4):686–689.

58. Gerdes CM, Kijowski R, Reeder SB. IDEAL imaging of the musculoskeletal system: robust water fat separation for uniform fat suppression, marrow evaluation, and cartilage imaging. AJR Am J Roentgenol 2007;189(5): W284–W291.

59. Jungius KP, Schmid MR, Zanetti M, Hodler J, Koch P, Pfirrmann CW. Cartilaginous defects of the femorotibial joint: accuracy of coronal short inversion time inversion-recovery MR sequence. Radiology 2006;240(2): 482–488.

60. Roemer FW, Guermazi A, Lynch JA, et al. Short tau inversion recovery and proton density-weighted fat suppressed sequences for the evaluation of osteoarthritis of the knee with a 1.0 T dedicated extremity MRI: development of a time-efficient sequence protocol. Eur Radiol 2005;15(5):978–987.

61. Link TM, Stahl R, Woertler K. Cartilage imaging: motivation, techniques, current and future significance. Eur Radiol 2007;17(5): 1135–1146.

62. Kijowski R, Davis KW, Woods MA, et al. Knee joint: comprehensive assessment with 3D isotropic resolution fast spin-echo MR imaging—diagnostic performance compared with that of conventional MR imaging at 3.0 T. Radiology 2009;252(2):486–495.

63. Ristow O, Steinbach L, Sabo G, et al. Isotropic 3D fast spin-echo imaging versus standard 2D imaging at 3.0 T of the knee—image quality and diagnostic performance. Eur Radiol 2009;19(5):1263–1272.

64. Friedrich KM, Reiter G, Kaiser B, et al. High-resolution cartilage imaging of the knee at 3T: Basic evaluation of modern isotropic 3D MR-sequences. Eur J Radiol 2010 Feb 5. [Epub ahead of print]

65. Disler DG, McCauley TR, Kelman CG, et al. Fat-suppressed three-dimensional spoiled gradient-echo MR imaging of hyaline cartilage defects in the knee: comparison with standard MR imaging and arthroscopy. AJR Am J Roentgenol 1996;167(1):127–132.

66. Disler DG, McCauley TR, Wirth CR, Fuchs MD. Detection of knee hyaline cartilage defects using fat-suppressed three-dimensional spoiled gradient-echo MR imaging: comparison with standard MR imaging and correlation with arthroscopy. AJR Am J Roentgenol 1995;165(2):377–382.

67. Disler DG. Fat-suppressed three-dimensional spoiled gradient-recalled MR imaging: assessment of articular and physeal hyaline cartilage. AJR Am J Roentgenol 1997; 169(4):1117–1123.

68. Wang SF, Cheng HC, Chang CY. Fat-suppressed three-dimensional fast spoiled gradient-recalled echo imaging: a modified FS 3D SPGR technique for assessment of patellofemoral joint chondromalacia. Clin Imaging 1999;23(3):177–180.

69. Eckstein F, Guermazi A, Roemer FW. Quantitative MR imaging of cartilage and trabecular bone in osteoarthritis. Radiol Clin North Am 2009;47(4):655–673.

70. Eckstein F, Buck RJ, Burstein D, et al. Precision of 3.0 Tesla quantitative magnetic resonance imaging of cartilage morphology in a multicentre clinical trial. Ann Rheum Dis 2008;67(12):1683–1688.

71. Crema MD, Guermazi A, Li L, et al. The association of prevalent medial meniscal pathology with cartilage loss in the medial tibiofemoral compartment over a 2-year period. Osteoarthritis Cartilage 2010;18(3):336–343.

72. Andreisek G, White LM, Sussman MS, et al. Quantitative MR imaging evaluation of the cartilage thickness and subchondral bone area in patients with ACL-reconstructions 7 years after surgery. Osteoarthritis Cartilage 2009;17(7):871–878.

73. Ruehm S, Zanetti M, Romero J, Hodler J. MRI of patellar articular cartilage: evaluation

of an optimized gradient echo sequence (3D-DESS). J Magn Reson Imaging 1998; 8(6):1246–1251.

74. Moriya S, Miki Y, Yokobayashi T, Ishikawa M. Three-dimensional double-echo steady-state (3D-DESS) magnetic resonance imaging of the knee: contrast optimization by adjusting flip angle. Acta Radiol 2009; 50(5):507–511.

75. Hardy PA, Recht MP, Piraino D, Thomasson D. Optimization of a dual echo in the steady state (DESS) free-precession sequence for imaging cartilage. J Magn Reson Imaging 1996;6(2):329–335.

76. Mosher TJ, Pruett SW. Magnetic resonance imaging of superficial cartilage lesions: role of contrast in lesion detection. J Magn Reson Imaging 1999;10(2):178–182.

77. Wirth W, Nevitt M, Hellio Le Graverand MP, et al. Sensitivity to change of cartilage morphometry using coronal FLASH, sagittal DESS, and coronal MPR DESS protocols—comparative data from the Osteoarthritis Initiative (OAI). Osteoarthritis Cartilage 2010;18(4):547–554.

78. Mohr A. The value of water-excitation 3D FLASH and fat-saturated PDw TSE MR imaging for detecting and grading articular cartilage lesions of the knee. Skeletal Radiol 2003;32(7):396–402.

79. Stahl R, Luke A, Ma CB, et al. Prevalence of pathologic findings in asymptomatic knees of marathon runners before and after a competition in comparison with physically active subjects-a 3.0 T magnetic resonance imaging study. Skeletal Radiol 2008;37(7): 627–638.

80. Masi JN, Sell CA, Phan C, et al. Cartilage MR imaging at 3.0 versus that at 1.5 T: preliminary results in a porcine model. Radiology 2005;236(1):140–150.

81. Barr C, Bauer JS, Malfair D, et al. MR imaging of the ankle at 3 Tesla and 1.5 Tesla: protocol optimization and application to cartilage, ligament and tendon pathology in cadaver specimens. Eur Radiol 2007;17(6):1518–1528.

82. Roemer FW, Kwoh CK, Hannon MJ, et al. Semiquantitative assessment of focal cartilage damage at 3T MRI: A comparative study of dual echo at steady state (DESS) and intermediate-weighted (IW) fat suppressed fast spin echo sequences. Eur J Radiol 2010 Sep 10. [Epub ahead of print]

83. Vasanawala SS, Hargreaves BA, Pauly JM, Nishimura DG, Beaulieu CF, Gold GE. Rapid musculoskeletal MRI with phase-sensitive steady-state free precession: comparison with routine knee MRI. AJR Am J Roentgenol 2005;184(5):1450–1455.

84. Duc SR, Koch P, Schmid MR, Horger W, Hodler J, Pfirrmann CW. Diagnosis of articular cartilage abnormalities of the knee: prospective clinical evaluation of a 3D water-excitation true FISP sequence. Radiology 2007;243(2):475–482.

85. Kornaat PR, Reeder SB, Koo S, et al. MR imaging of articular cartilage at 1.5T and 3.0T: comparison of SPGR and SSFP sequences. Osteoarthritis Cartilage 2005;13(4):338–344.

86. Duc SR, Pfirrmann CW, Koch PP, Zanetti M, Hodler J. Internal knee derangement assessed with 3-minute three-dimensional isovoxel true FISP MR sequence: preliminary study. Radiology 2008;246(2):526–535.

87. Kijowski R, Blankenbaker DG, Klaers JL, Shinki K, De Smet AA, Block WF. Vastly undersampled isotropic projection steady-state free precession imaging of the knee: diagnostic performance compared with conventional MR. Radiology 2009;251(1): 185–194.

88. Yoshioka H, Stevens K, Hargreaves BA, et al. Magnetic resonance imaging of articular cartilage of the knee: comparison between fat-suppressed three-dimensional SPGR imaging, fat-suppressed FSE imaging, and fat-suppressed three-dimensional DEFT imaging, and correlation with arthroscopy. J Magn Reson Imaging 2004;20(5):857–864.

89. Gold GE, Fuller SE, Hargreaves BA, Stevens KJ, Beaulieu CF. Driven equilibrium magnetic resonance imaging of articular cartilage: initial clinical experience. J Magn Reson Imaging 2005;21(4):476–481.

90. Peterfy CG, Gold G, Eckstein F, Cicuttini F, Dardzinski B, Stevens R. MRI protocols for whole-organ assessment of the knee in osteoarthritis. Osteoarthritis Cartilage 2006;14 (Suppl A):A95–A111.

91. Folkesson J, Dam EB, Olsen OF, Christiansen C. Accuracy evaluation of automatic quantification of the articular cartilage surface curvature from MRI. Acad Radiol 2007;14(10):1221–1228.

92. Folkesson J, Dam EB, Olsen OF, Pettersen PC, Christiansen C. Segmenting articular cartilage automatically using a voxel classification approach. IEEE Trans Med Imaging 2007; 26(1):106–115.

93. Kladny B, Glückert K, Swoboda B, Beyer W, Weseloh G. Comparison of low-field (0.2 Tesla) and high-field (1.5 Tesla) magnetic resonance imaging of the knee joint. Arch Orthop Trauma Surg 1995;114(5):281–286.

94. Woertler K, Strothmann M, Tombach B, Reimer P. Detection of articular cartilage lesions: experimental evaluation of low- and high-field-strength MR imaging at 0.18 and 1.0 T. J Magn Reson Imaging 2000;11(6): 678–685.

95. Roemer FW, Lynch JA, Niu J, et al. A comparison of dedicated 1.0 T extremity MRI vs large-bore 1.5 T MRI for semiquantitative whole organ assessment of osteoarthritis: the MOST study. Osteoarthritis Cartilage 2010;18(2):168–174.

96. Salzmann GM, Paul J, Bauer JS, et al. T2 assessment and clinical outcome following autologous matrix-assisted chondrocyte and osteochondral autograft transplantation. Osteoarthritis Cartilage 2009;17(12):1576–1582.

97. Trattnig S, Mamisch TC, Pinker K, et al. Differentiating normal hyaline cartilage from post-surgical repair tissue using fast gradient echo imaging in delayed gadolinium-enhanced MRI (dGEMRIC) at 3 Tesla. Eur Radiol 2008; 18(6):1251–1259.

98. Link TM, Sell CA, Masi JN, et al. 3.0 vs 1.5 T MRI in the detection of focal cartilage pathology—ROC analysis in an experimental model. Osteoarthritis Cartilage 2006;14(1): 63–70.

99. Kijowski R, Blankenbaker DG, Davis KW, Shinki K, Kaplan LD, De Smet AA. Comparison of 1.5- and 3.0-T MR imaging for evaluating the articular cartilage of the knee joint. Radiology 2009;250(3):839–848.

100. Bauer JS, Krause SJ, Ross CJ, et al. Volumetric cartilage measurements of porcine knee at 1.5-T and 3.0-T MR imaging: evaluation of precision and accuracy. Radiology 2006;241(2):399–406.

101. Stahl R, Krug R, Kelley DA, et al. Assessment of cartilage-dedicated sequences at ultra-high-field MRI: comparison of imaging performance and diagnostic confidence between 3.0 and 7.0 T with respect to osteoarthritis-induced changes at the knee joint. Skeletal Radiol 2009;38(8):771–783.

102. Wang L, Wu Y, Chang G, et al. Rapid isotropic 3D-sodium MRI of the knee joint in vivo at 7T. J Magn Reson Imaging 2009; 30(3):606–614.

103. Krug R, Carballido-Gamio J, Banerjee S, et al. In vivo bone and cartilage MRI using fully-balanced steady-state free-precession at 7 tesla. Magn Reson Med 2007;58(6): 1294–1298.

104. Logan MC, Williams A, Lavelle J, Gedroyc W, Freeman M. Tibiofemoral kinematics following successful anterior cruciate ligament reconstruction using dynamic multiple resonance imaging. Am J Sports Med 2004; 32(4):984–992.

105. Nishii T, Kuroda K, Matsuoka Y, Sahara T, Yoshikawa H. Change in knee cartilage T2

in response to mechanical loading. J Magn Reson Imaging 2008;28(1):175–180.

106. Eckstein F, Ateshian G, Burgkart R, et al. Proposal for a nomenclature for magnetic resonance imaging based measures of articular cartilage in osteoarthritis. Osteoarthritis Cartilage 2006;14(10):974–983.

107. Solloway S, Hutchinson CE, Waterton JC, Taylor CJ. The use of active shape models for making thickness measurements of articular cartilage from MR images. Magn Reson Med 1997;37(6):943–952.

108. Stammberger T, Eckstein F, Michaelis M, Englmeier KH, Reiser M. Interobserver reproducibility of quantitative cartilage measurements: comparison of B-spline snakes and manual segmentation. Magn Reson Imaging 1999;17(7):1033–1042.

109. Cohen ZA, McCarthy DM, Kwak SD, et al. Knee cartilage topography, thickness, and contact areas from MRI: in-vitro calibration and in-vivo measurements. Osteoarthritis Cartilage 1999;7(1):95–109.

110. Kauffmann C, Gravel P, Godbout B, et al. Computer-aided method for quantification of cartilage thickness and volume changes using MRI: validation study using a synthetic model. IEEE Trans Biomed Eng 2003; 50(8):978–988.

111. Hohe J, Faber S, Stammberger T, Reiser M, Englmeier KH, Eckstein F. A technique for 3D in vivo quantification of proton density and magnetization transfer coefficients of knee joint cartilage. Osteoarthritis Cartilage 2000;8(6):426–433.

112. Qazi AA, Folkesson J, Pettersen PC, Karsdal MA, Christiansen C, Dam EB. Separation of healthy and early osteoarthritis by automatic quantification of cartilage homogeneity. Osteoarthritis Cartilage 2007;15(10): 1199–1206.

113. Burgkart R, Glaser C, Hinterwimmer S, et al. Feasibility of T and Z scores from magnetic resonance imaging data for quantification of cartilage loss in osteoarthritis. Arthritis Rheum 2003;48(10):2829–2835.

114. von Eisenhart-Rothe R, Graichen H, Hudelmaier M, Vogl T, Sharma L, Eckstein F. Femorotibial and patellar cartilage loss in patients prior to total knee arthroplasty, heterogeneity, and correlation with alignment of the knee. Ann Rheum Dis 2006;65(1):69–73.

115. Otterness IG, Eckstein F. Women have thinner cartilage and smaller joint surfaces than men after adjustment for body height and weight. Osteoarthritis Cartilage 2007; 15(6):666–672.

116. Wang Y, Ding C, Wluka AE, et al. Factors affecting progression of knee cartilage defects in normal subjects over 2 years. Rheumatology (Oxford) 2006;45(1):79–84.

117. Eckstein F, Hudelmaier M, Cahue S, Marshall M, Sharma L. Medial-to-lateral ratio of tibiofemoral subchondral bone area is adapted to alignment and mechanical load. Calcif Tissue Int 2009;84(3):186–194.

118. Cohen ZA, Mow VC, Henry JH, Levine WN, Ateshian GA. Templates of the cartilage layers of the patellofemoral joint and their use in the assessment of osteoarthritic cartilage damage. Osteoarthritis Cartilage 2003;11(8):569–579.

119. Buck RJ, Wyman BT, Le Graverand MP, et al. Does the use of ordered values of subregional change in cartilage thickness improve the detection of disease progression in longitudinal studies of osteoarthritis? Arthritis Rheum 2009;61(7):917–924.

120. Eckstein F, Burstein D, Link TM. Quantitative MRI of cartilage and bone: degenerative changes in osteoarthritis. NMR Biomed 2006;19(7):822–854.

121. Inglis D, Pui M, Ioannidis G, et al. Accuracy and test-retest precision of quantitative cartilage morphology on a 1.0 T peripheral magnetic resonance imaging system. Osteoarthritis Cartilage 2007;15(1):110–115.

122. Dam EB, Folkesson J, Pettersen PC, Christiansen C. Automatic morphometric cartilage quantification in the medial tibial plateau from MRI for osteoarthritis grading. Osteoarthritis Cartilage 2007;15(7): 808–818.

123. Eckstein F, Charles HC, Buck RJ, et al. Accuracy and precision of quantitative assessment of cartilage morphology by magnetic resonance imaging at 3.0T. Arthritis Rheum 2005;52(10):3132–3136.

124. Eckstein F, Kunz M, Hudelmaier M, et al. Impact of coil design on the contrast-to-noise ratio, precision, and consistency of quantitative cartilage morphometry at 3 Tesla: a pilot study for the osteoarthritis initiative. Magn Reson Med 2007;57(2):448–454.

125. Eckstein F, Kunz M, Schutzer M, et al. Two year longitudinal change and test-retest-precision of knee cartilage morphology in a pilot study for the osteoarthritis initiative. Osteoarthritis Cartilage 2007;15(11):1326–1332.

126. Eckstein F, Maschek S, Wirth W, et al. One year change of knee cartilage morphology in the first release of participants from the Osteoarthritis Initiative progression subcohort: association with sex, body mass index, symptoms and radiographic osteoarthritis status. Ann Rheum Dis 2009;68(5):674–679.

127. Eckstein F, Wirth W, Hudelmaier M, et al. Patterns of femorotibial cartilage loss in knees with neutral, varus, and valgus alignment. Arthritis Rheum 2008;59(11):1563–1570.

128. Hunter DJ, Niu J, Zhang Y, et al. Change in cartilage morphometry: a sample of the progression cohort of the Osteoarthritis Initiative. Ann Rheum Dis 2009;68(3):349–356.

129. Pelletier JP, Raynauld JP, Berthiaume MJ, et al. Risk factors associated with the loss of cartilage volume on weight-bearing areas in knee osteoarthritis patients assessed by quantitative magnetic resonance imaging: a longitudinal study. Arthritis Res Ther 2007; 9(4):R74.

130. Gandy SJ, Dieppe PA, Keen MC, Maciewicz RA, Watt I, Waterton JC. No loss of cartilage volume over three years in patients with knee osteoarthritis as assessed by magnetic resonance imaging. Osteoarthritis Cartilage 2002;10(12):929–937.

131. Wluka AE, Stuckey S, Snaddon J, Cicuttini FM. The determinants of change in tibial cartilage volume in osteoarthritic knees. Arthritis Rheum 2002;46(8):2065–2072.

132. Cicuttini FM, Wluka AE, Wang Y, Stuckey SL. Longitudinal study of changes in tibial and femoral cartilage in knee osteoarthritis. Arthritis Rheum 2004;50(1):94–97.

133. Raynauld JP, Martel-Pelletier J, Berthiaume MJ, et al. Quantitative magnetic resonance imaging evaluation of knee osteoarthritis progression over two years and correlation with clinical symptoms and radiologic changes. Arthritis Rheum 2004; 50(2):476–487.

134. Berthiaume MJ, Raynauld JP, Martel-Pelletier J, et al. Meniscal tear and extrusion are strongly associated with progression of symptomatic knee osteoarthritis as assessed by quantitative magnetic resonance imaging. Ann Rheum Dis 2005;64(4):556–563.

135. Raynauld JP, Martel-Pelletier J, Berthiaume MJ, et al. Long term evaluation of disease progression through the quantitative magnetic resonance imaging of symptomatic knee osteoarthritis patients: correlation with clinical symptoms and radiographic changes. Arthritis Res Ther 2006; 8(1):R21.

136. Wluka AE, Forbes A, Wang Y, Hanna F, Jones G, Cicuttini FM. Knee cartilage loss in symptomatic knee osteoarthritis over 4.5 years. Arthritis Res Ther 2006;8(4):R90.

137. Bruyere O, Genant H, Kothari M, et al. Longitudinal study of magnetic resonance imaging and standard X-rays to assess disease progression in osteoarthritis. Osteoarthritis Cartilage 2007;15(1):98–103.

138. Wirth W, Hellio Le Graverand MP, Wyman BT, et al. Regional analysis of fem-

orotibial cartilage loss in a subsample from the Osteoarthritis Initiative progression subcohort. Osteoarthritis Cartilage 2009;17(3):291–297.

139. Frobell RB, Le Graverand MP, Buck R, et al. The acutely ACL injured knee assessed by MRI: changes in joint fluid, bone marrow lesions, and cartilage during the first year. Osteoarthritis Cartilage 2009;17(2):161–167.

140. Watson PJ, Carpenter TA, Hall LD, Tyler JA. Cartilage swelling and loss in a spontaneous model of osteoarthritis visualized by magnetic resonance imaging. Osteoarthritis Cartilage 1996;4(3):197–207.

141. Calvo E, Palacios I, Delgado E, et al. High-resolution MRI detects cartilage swelling at the early stages of experimental osteoarthritis. Osteoarthritis Cartilage 2001;9(5):463–472.

142. Adams ME, Brandt KD. Hypertrophic repair of canine articular cartilage in osteoarthritis after anterior cruciate ligament transection. J Rheumatol 1991;18(3):428–435.

143. Vignon E, Arlot M, Hartmann D, Moyen B, Ville G. Hypertrophic repair of articular cartilage in experimental osteoarthrosis. Ann Rheum Dis 1983;42(1):82–88.

144. Cicuttini F, Wluka A, Wang Y, Stuckey S. The determinants of change in patella cartilage volume in osteoarthritic knees. J Rheumatol 2002;29(12):2615–2619.

145. Sharma L, Eckstein F, Song J, et al. Relationship of meniscal damage, meniscal extrusion, malalignment, and joint laxity to subsequent cartilage loss in osteoarthritic knees. Arthritis Rheum 2008;58(6):1716–1726.

146. Cicuttini F, Wluka A, Hankin J, Wang Y. Longitudinal study of the relationship between knee angle and tibiofemoral cartilage volume in subjects with knee osteoarthritis. Rheumatology (Oxford) 2004;43(3):321–324.

147. Raynauld JP, Martel-Pelletier J, Berthiaume MJ, et al. Correlation between bone lesion changes and cartilage volume loss in patients with osteoarthritis of the knee as assessed by quantitative magnetic resonance imaging over a 24-month period. Ann Rheum Dis 2008;67(5):683–688.

148. Wluka AE, Hanna F, Davies-Tuck M, et al. Bone marrow lesions predict increase in knee cartilage defects and loss of cartilage volume in middle-aged women without knee pain over 2 years. Ann Rheum Dis 2009;68(6):850–855.

149. Ding C, Cicuttini F, Scott F, Boon C, Jones G. Association of prevalent and incident knee cartilage defects with loss of tibial and patellar cartilage: a longitudinal study. Arthritis Rheum 2005;52(12):3918–3927.

150. Wluka AE, Ding C, Jones G, Cicuttini FM. The clinical correlates of articular cartilage defects in symptomatic knee osteoarthritis: a prospective study. Rheumatology (Oxford) 2005;44(10):1311–1316.

151. Ding C, Cicuttini F, Blizzard L, Jones G. Smoking interacts with family history with regard to change in knee cartilage volume and cartilage defect development. Arthritis Rheum 2007;56(5):1521–1528.

152. Ding C, Martel-Pelletier J, Pelletier JP, et al. Two-year prospective longitudinal study exploring the factors associated with change in femoral cartilage volume in a cohort largely without knee radiographic osteoarthritis. Osteoarthritis Cartilage 2008;16(4):443–449.

153. Shapiro EM, Borthakur A, Gougoutas A, Reddy R. 23Na MRI accurately measures fixed charge density in articular cartilage. Magn Reson Med 2002;47(2):284–291.

154. Welsch GH, Mamisch TC, Hughes T, et al. In vivo biochemical 7.0 Tesla magnetic resonance: preliminary results of dGEMRIC, zonal T2, and T2* mapping of articular cartilage. Invest Radiol 2008;43(9):619–626.

155. Bashir A, Gray ML, Burstein D. Gd-DTPA2- as a measure of cartilage degradation. Magn Reson Med 1996;36(5):665–673.

156. Bashir A, Gray ML, Boutin RD, Burstein D. Glycosaminoglycan in articular cartilage: in vivo assessment with delayed Gd(DTPA)(2-)-enhanced MR imaging. Radiology 1997;205(2):551–558.

157. Kim YJ, Jaramillo D, Millis MB, Gray ML, Burstein D. Assessment of early osteoarthritis in hip dysplasia with delayed gadolinium-enhanced magnetic resonance imaging of cartilage. J Bone Joint Surg Am 2003;85-A(10):1987–1992.

158. Roos EM, Dahlberg L. Positive effects of moderate exercise on glycosaminoglycan content in knee cartilage: a four-month, randomized, controlled trial in patients at risk of osteoarthritis. Arthritis Rheum 2005;52(11):3507–3514.

159. Fleming BC, Oksendahl HL, Mehan WA, et al. Delayed gadolinium-enhanced MR imaging of cartilage (dGEMRIC) following ACL injury. Osteoarthritis Cartilage 2010;18(5):662–667.

160. Jessel RH, Zilkens C, Tiderius C, Dudda M, Mamisch TC, Kim YJ. Assessment of osteoarthritis in hips with femoroacetabular impingement using delayed gadolinium enhanced MRI of cartilage. J Magn Reson Imaging 2009;30(5):1110–1115.

161. Duvvuri U, Reddy R, Patel SD, Kaufman JH, Kneeland JB, Leigh JS. T1rho-relaxation in articular cartilage: effects of enzymatic degradation. Magn Reson Med 1997;38(6):863–867.

162. Akella SV, Regatte RR, Gougoutas AJ, et al. Proteoglycan-induced changes in T1rho-relaxation of articular cartilage at 4T. Magn Reson Med 2001;46(3):419–423.

163. Menezes NM, Gray ML, Hartke JR, Burstein D. T2 and T1rho MRI in articular cartilage systems. Magn Reson Med 2004;51(3):503–509.

164. Regatte RR, Akella SV, Wheaton AJ, et al. 3D-T1rho-relaxation mapping of articular cartilage: in vivo assessment of early degenerative changes in symptomatic osteoarthritic subjects. Acad Radiol 2004;11(7):741–749.

165. Regatte RR, Akella SV, Lonner JH, Kneeland JB, Reddy R. T1rho relaxation mapping in human osteoarthritis (OA) cartilage: comparison of T1rho with T2. J Magn Reson Imaging 2006;23(4):547–553.

166. Mlynárik V, Szomolányi P, Toffanin R, Vittur F, Trattnig S. Transverse relaxation mechanisms in articular cartilage. J Magn Reson 2004;169(2):300–307.

167. Li X, Benjamin Ma C, Link TM, et al. In vivo T(1rho) and T(2) mapping of articular cartilage in osteoarthritis of the knee using 3 T MRI. Osteoarthritis Cartilage 2007;15(7):789–797.

168. Li X, Han ET, Busse RF, Majumdar S. In vivo T(1rho) mapping in cartilage using 3D magnetization-prepared angle-modulated partitioned k-space spoiled gradient echo snapshots (3D MAPSS). Magn Reson Med 2008;59(2):298–307.

169. Pakin SK, Schweitzer ME, Regatte RR. 3D-T1rho quantitation of patellar cartilage at 3.0T. J Magn Reson Imaging 2006;24(6):1357–1363.

170. Pakin SK, Xu J, Schweitzer ME, Regatte RR. Rapid 3D-T1rho mapping of the knee joint at 3.0T with parallel imaging. Magn Reson Med 2006;56(3):563–571.

171. Li X, Han ET, Ma CB, Link TM, Newitt DC, Majumdar S. In vivo 3T spiral imaging based multi-slice T(1rho) mapping of knee cartilage in osteoarthritis. Magn Reson Med 2005;54(4):929–936.

172. Majumdar S, Li X, Blumenkrantz G, et al. MR imaging and early cartilage degeneration and strategies for monitoring regeneration. J Musculoskelet Neuronal Interact 2006;6(4):382–384.

173. Shapiro EM, Borthakur A, Dandora R, Kriss A, Leigh JS, Reddy R. Sodium visibility and quantitation in intact bovine articular cartilage using high field (23)Na MRI and MRS. J Magn Reson 2000;142(1):24–31.

174. Borthakur A, Shapiro EM, Beers J, Kudchodkar S, Kneeland JB, Reddy R. Sensitivity of MRI to proteoglycan depletion in cartilage: comparison of sodium and proton MRI. Osteoarthritis Cartilage 2000;8(4):288–293.

175. Mosher TJ, Dardzinski BJ. Cartilage MRI T2 relaxation time mapping: overview and applications. Semin Musculoskelet Radiol 2004;8(4):355–368.

176. Smith HE, Mosher TJ, Dardzinski BJ, et al. Spatial variation in cartilage T2 of the knee. J Magn Reson Imaging 2001;14(1):50–55.

177. Mosher TJ, Smith HE, Collins C, et al. Change in knee cartilage T2 at MR imaging after running: a feasibility study. Radiology 2005;234(1):245–249.

178. Stanisz GJ, Odrobina EE, Pun J, et al. T1, T2 relaxation and magnetization transfer in tissue at 3T. Magn Reson Med 2005;54(3):507–512.

179. Mosher TJ, Dardzinski BJ, Smith MB. Human articular cartilage: influence of aging and early symptomatic degeneration on the spatial variation of T2—preliminary findings at 3 T. Radiology 2000;214(1):259–266.

180. Dunn TC, Lu Y, Jin H, Ries MD, Majumdar S. T2 relaxation time of cartilage at MR imaging: comparison with severity of knee osteoarthritis. Radiology 2004;232(2):592–598.

181. Stehling C, Liebl H, Krug R, et al. Patellar cartilage: T2 values and morphologic abnormalities at 3.0-T MR imaging in relation to physical activity in asymptomatic subjects from the osteoarthritis initiative. Radiology 2010;254(2):509–520.

182. Knutsen G, Drogset JO, Engebretsen L, et al. A randomized trial comparing autologous chondrocyte implantation with microfracture. Findings at five years. J Bone Joint Surg Am 2007;89(10):2105–2112.

183. Gudas R, Kalesinskas RJ, Kimtys V, et al. A prospective randomized clinical study of mosaic osteochondral autologous transplantation versus microfracture for the treatment of osteochondral defects in the knee joint in young athletes. Arthroscopy 2005;21(9):1066–1075.

184. Brittberg M, Lindahl A, Nilsson A, Ohlsson C, Isaksson O, Peterson L. Treatment of deep cartilage defects in the knee with autologous chondrocyte transplantation. N Engl J Med 1994;331(14):889–895.

185. Trattnig S, Domayer S, Welsch GW, Mosher T, Eckstein F. MR imaging of cartilage and its repair in the knee—a review. Eur Radiol 2009;19(7):1582–1594.

186. Welsch GH, Mamisch TC, Quirbach S, Zak L, Marlovits S, Trattnig S. Evaluation and comparison of cartilage repair tissue of the patella and medial femoral condyle by using morphological MRI and biochemical zonal T2 mapping. Eur Radiol 2009;19(5):1253–1262.

187. Welsch GH, Trattnig S, Domayer S, Marlovits S, White LM, Mamisch TC. Multimodal approach in the use of clinical scoring, morphological MRI and biochemical T2-mapping and diffusion-weighted imaging in their ability to assess differences between cartilage repair tissue after microfracture therapy and matrix-associated autologous chondrocyte transplantation: a pilot study. Osteoarthritis Cartilage 2009;17(9):1219–1227.

188. Marlovits S, Striessnig G, Resinger CT, et al. Definition of pertinent parameters for the evaluation of articular cartilage repair tissue with high-resolution magnetic resonance imaging. Eur J Radiol 2004;52(3):310–319.

189. Marlovits S, Singer P, Zeller P, Mandl I, Haller J, Trattnig S. Magnetic resonance observation of cartilage repair tissue (MOCART) for the evaluation of autologous chondrocyte transplantation: determination of interobserver variability and correlation to clinical outcome after 2 years. Eur J Radiol 2006;57(1):16–23.

190. Choi YS, Potter HG, Chun TJ. MR imaging of cartilage repair in the knee and ankle. RadioGraphics 2008;28(4):1043–1059.

191. Domayer SE, Kutscha-Lissberg F, Welsch G, et al. T2 mapping in the knee after microfracture at 3.0 T: correlation of global T2 values and clinical outcome - preliminary results. Osteoarthritis Cartilage 2008;16(8):903–908.

192. Ebert JR, Robertson WB, Lloyd DG, Zheng MH, Wood DJ, Ackland T. Traditional vs accelerated approaches to post-operative rehabilitation following matrix-induced autologous chondrocyte implantation (MACI): comparison of clinical, biomechanical and radiographic outcomes. Osteoarthritis Cartilage 2008;16(10):1131–1140.

193. Welsch GH, Zak L, Mamisch TC, Resinger C, Marlovits S, Trattnig S. Three-dimensional magnetic resonance observation of cartilage repair tissue (MOCART) score assessed with an isotropic three-dimensional true fast imaging with steady-state precession sequence at 3.0 Tesla. Invest Radiol 2009;44(9):603–612.

194. Kurkijärvi JE, Mattila L, Ojala RO, et al. Evaluation of cartilage repair in the distal femur after autologous chondrocyte transplantation using T2 relaxation time and dGEMRIC. Osteoarthritis Cartilage 2007;15(4):372–378.

195. Gillis A, Bashir A, McKeon B, Scheller A, Gray ML, Burstein D. Magnetic resonance imaging of relative glycosaminoglycan distribution in patients with autologous chondrocyte transplants. Invest Radiol 2001;36(12):743–748.

196. Trattnig S, Marlovits S, Gebetsroither S, et al. Three-dimensional delayed gadolinium-enhanced MRI of cartilage (dGEMRIC) for in vivo evaluation of reparative cartilage after matrix-associated autologous chondrocyte transplantation at 3.0T: Preliminary results. J Magn Reson Imaging 2007;26(4):974–982.

197. Pinker K, Szomolanyi P, Welsch GC, et al. Longitudinal evaluation of cartilage composition of matrix-associated autologous chondrocyte transplants with 3-T delayed gadolinium-enhanced MRI of cartilage. AJR Am J Roentgenol 2008;191(5):1391–1396.

198. Nehrer S, Minas T. Treatment of articular cartilage defects. Invest Radiol 2000;35(10):639–646.

199. Tins BJ, McCall IW, Takahashi T, et al. Autologous chondrocyte implantation in knee joint: MR imaging and histologic features at 1-year follow-up. Radiology 2005;234(2):501–508.

200. Minas T, Nehrer S. Current concepts in the treatment of articular cartilage defects. Orthopedics 1997;20(6):525–538.

201. Ghivizzani SC, Oligino TJ, Robbins PD, Evans CH. Cartilage injury and repair. Phys Med Rehabil Clin N Am 2000;11(2):289–307, vi.

202. Welsch GH, Mamisch TC, Domayer SE, et al. Cartilage T2 assessment at 3-T MR imaging: in vivo differentiation of normal hyaline cartilage from reparative tissue after two cartilage repair procedures—initial experience. Radiology 2008;247(1):154–161.

203. Friedrich KM, Mamisch TC, Plank C, et al. Diffusion-weighted imaging for the follow-up of patients after matrix-associated autologous chondrocyte transplantation. Eur J Radiol 2010;73(3):622–628.

204. Mamisch TC, Menzel MI, Welsch GH, et al. Steady-state diffusion imaging for MR in-vivo evaluation of reparative cartilage after matrix-associated autologous chondrocyte transplantation at 3 tesla—preliminary results. Eur J Radiol 2008;65(1):72–79.

205. Quirbach S, Trattnig S, Marlovits S, et al. Initial results of in vivo high-resolution morphological and biochemical cartilage imaging of patients after matrix-associated autologous chondrocyte transplantation (MACT) of the ankle. Skeletal Radiol 2009;38(8):751–760.

206. Keen HI, Wakefield RJ, Conaghan PG. A systematic review of ultrasonography in osteoarthritis. Ann Rheum Dis 2009;68(5):611–619.

207. Schmidt WA, Völker L, Zacher J, Schläfke M, Ruhnke M, Gromnica-Ihle E. Colour Doppler ultrasonography to detect pannus in knee joint synovitis. Clin Exp Rheumatol 2000;18(4):439–444.

208. Wakefield RJ, Gibbon WW, Emery P. The current status of ultrasonography in rheumatology. Rheumatology (Oxford) 1999;38(3):195–198.

209. Roemer FW, van Holsbeeck M, Genant HK. Musculoskeletal ultrasound in rheumatology: a radiologic perspective. Arthritis Rheum 2005;53(4):491–493.

210. Qvistgaard E, Kristoffersen H, Terslev L, Danneskiold-Samsøe B, Torp-Pedersen S, Bliddal H. Guidance by ultrasound of intraarticular injections in the knee and hip joints. Osteoarthritis Cartilage 2001;9(6):512–517.

211. Monteforte P, Rovetta G. Sonographic assessment of soft tissue alterations in osteoarthritis of the knee. Int J Tissue React 1999;21(1):19–23.

212. Iagnocco A, Coari G. Usefulness of high resolution US in the evaluation of effusion in osteoarthritic first carpometacarpal joint. Scand J Rheumatol 2000;29(3):170–173.

213. Hunter DJ, Lo GH. The management of osteoarthritis: an overview and call to appropriate conservative treatment. Med Clin North Am 2009;93(1):127–143, xi.

214. Katz JN, Mahomed NN, Baron JA, et al. Association of hospital and surgeon procedure volume with patient-centered outcomes of total knee replacement in a population-based cohort of patients age 65 years and older. Arthritis Rheum 2007;56(2):568–574.

215. American College of Rheumatology Subcommittee on Osteoarthritis Guidelines. Recommendations for the medical management of osteoarthritis of the hip and knee: 2000 update. Arthritis Rheum 2000 43(9):1905–1915.

216. Zhang W, Doherty M, Arden N, et al. EULAR evidence based recommendations for the management of hip osteoarthritis: report of a task force of the EULAR Standing Committee for International Clinical Studies Including Therapeutics (ESCISIT). Ann Rheum Dis 2005;64(5):669–681.

217. Zhang W, Moskowitz RW, Nuki G, et al. OARSI recommendations for the management of hip and knee osteoarthritis, Part II: OARSI evidence-based, expert consensus guidelines. Osteoarthritis Cartilage 2008;16(2):137–162.